Another look through the microscope – Locally resolved electronic absorption spectra of silicate minerals measured in a microscope- spectrometer

Nový pohled mikroskopem – lokálně rozlišená elektronová absorbční spektra silikátů měřená mikroskopem-spektrometrem

(15 text-figs, 3 tabs)

KLAUS LANGER

Institute of Applied Geosciences I, Technical University of Berlin, D–10623 Berlin, Germany

Concepts of absorption spectroscopy in the UV/VIS/NIR and of excitations of electronic transitions in oxygen-based minerals in this spectral range are outlined. Absorption of energy in this range excites transitions in the electronic systems of ligands and central ion in polyhedra, LM-CT, in the electronic systems of two $3d^N$-ions with different valence and allocated in interconnected polyhedra, MM-CT and, finally, between energy states of the $3d^N$-ions themselves, dd-sa and dd-sf. Theoretical aspects of such transitions and their evaluation, to obtain much information useful in crystal chemistry and crystal physics of minerals, is briefly sketched.

To overcome difficulties related to the often occurring neccessity of scanning spectra on small crystals, small optically clear parts of larger crystals, or through small apertures of special devices as high-pressure DAC-cells, high-temperature cells *etc.*, microscope-spectrometric methods were developed that are discussed here. They allow measurement on crystal spots down to about 5 μm in diameter, of polarized single-crystal spectra in the wide spectral range from 40000 to 5000 cm^{-1} (250 to 2000 nm) at ambient conditions and in a pressure range up to 20 GPa or at temperatures between about 100 and 900 °K.

The paper presents examples of applications of such methods in the fields of mineral colour, band assignements in complex minerals by the study of chemically simple synthetic equivalents, of mineral analysis including Fe^{2+}, Fe^{3+}, of intra- and intercrystalline $3d^N$-ion distribution and of the analysis of local structural properties of $3d^N$-ion centered polyhedra. Local structural peculiarities cannot be elucidated by diffraction methods of structural research, as these methods are crystal averaging and do not individually see *e. g.* an $3d^N$-ion centered polyhedron in a mineral structure. In this field, the paper discusses the analysis of fO_2–T-dependent formation of Fe^{3+}-bearing point defects in fayalite and olivines. Here, the results can be used to estimate the oxygen fugacity of olivine formation in nature. Further, the evaluation of local mean $3d^N$-ion – ligand distances of individual $3d^N$-ion centered polyhedra, and determinations of polyhedral compression as well as polyhedral thermal expansion are dealt with.

Key words: Microscope-spectrometry, silicate minerals, electronic transitions, local structural properties, ligand-field theory

The present paper is dedicated to Dr. sci. Pavel Povondra at the occasion of his 75th birthday. This Dedication is a pleasure and honour for the author as the two of us travelled June 16th to 19th, 1970, together from Bochum to Frankfurt to visit the ACHEMA. Here, we saw a Zeiss instrument which, after functional alterations, some of which were induced by Pavel's questions, was 1971 ready to start the microscope-spectrometric work sketched here.

Introduction

Scholars in geosciences become early familiar with the polarizing microscope as the most important tool for orthoscopic direct observation of geoscientific objects and for orthoscopic or conoscopic observation of the effects of refraction of light in mineral crystals.

What is not known to many geoscientists is that a polarizing microscope, when equipped with an appropriate monochromator and photometric device, can be used to measure polarized single-crystal spectra (Langer – Abu-Eid 1977, Piller 1977, Langer – Frentrup 1979, Langer 1988) in a broad spectral range from the ultraviolet down to the infrared. In the case of electronic absorption spectra, which are recorded in the UV/VIS/NIR spectral ranges, local resolutions down to diameters of 3.5 μm may be achieved in favourable spectra ranges, as will be shown in this paper.

This opens the possibility to measure polarized electronic spectra on very small natural or synthetic crystals the spectra of which could otherwise only be measured by powder-remission methods (Kortüm 1969). This latter method cannot provide the information which can be extracted from band polarizations and which is only achieved by spectroscopy on oriented single crystals using lineraly polarized radiation. Also, microscope-spectrometry opens the posibility to measure single crystal spectra on small optically clear spots or along profiles in larger crystals as well as through small apertures, typical *e. g.* of diamond anvil high-pressure cells or cells for measurements at different temperatures.

As electronic spectra allow for the extraction of geoscientifically important information on minerals, as shown below, high local resolution is of high importance in this field. Here, it should be pointed out only that electronic spectroscopy elucidates local structural properties, which are typical for the active centers just in resonance with the exciting radiation. As such local properties cannot be detected by the crystal-averaging diffraction methods of structural research, absorption spectroscopic methods are powerfully complementing the diffraction methods.

There are currently only five groups in the world (except for the author's group) working by microscope-specrometry of electronic absorption spectra of minerals (Platonov and coworkers, Kyiv; Wildner and coworkers, Vienna; Keppler and coworkers, Bayreuth; Hålenius, Stockholm; Amthauer and coworkers, Salzburg). Because of the many applications in the geosciences, such methods need to be propagated. Therefore, it is the aim of this paper to present and discuss three essential aspects of this field: First, a theoretical sketch of what information can be extracted from electronic absorption spectra; second, the microscope-spectrometric methods themselves; and third, some recent applications and results of microscope-spectrometry.

1. Information to be extracted from electronic absorption spectra – a sketch of theoretical aspects

1.1 Spectral ranges and units in absorption spectra, characteristics of absorption bands

Fig. 1 displays the range of the electromagnetical spectrum in the spectral range 40000 to 0 [cm^{-1}]. This corresponds to the wavelenth range of 250 to ∞ [nm] and includes the low-energy UV, visible, near-infrared, infrared and far-infrared regions as shown in Fig. 1. It may be recalled that the wavenumber in [cm^{-1}] is an unit of the energy, E, of the electromagnetic radiation which is proportional to the inverse, $1/\lambda$, of its wavelength, λ:

$$E = h \cdot \nu \quad (1)$$

with $c_o = \lambda \cdot \nu$ (2)

to obtain $E = h \cdot c_o + (1/\lambda)$ (3)

or $1/\lambda = E / h \cdot c_o$ (3a)

where h = Planck's constant, c_o = velocity of light in vacuum, l = wavelength, v = frequency of the electromagnetic radiation. Choosing the proper units in the [cgs] system or corresponding other systems of units, we obain 1/l, the wavenumber, as

$$1\ cm^{-1} = 1.2397 \cdot 10^{-4}\ eV = 4.7442 \cdot 10^{-24}\ cal = 1.9863 \cdot 10^{-23} \quad (4)$$

To recalculate these energies per g-atom or per mole, the conversion factors are multiplied by Avogadro's num-

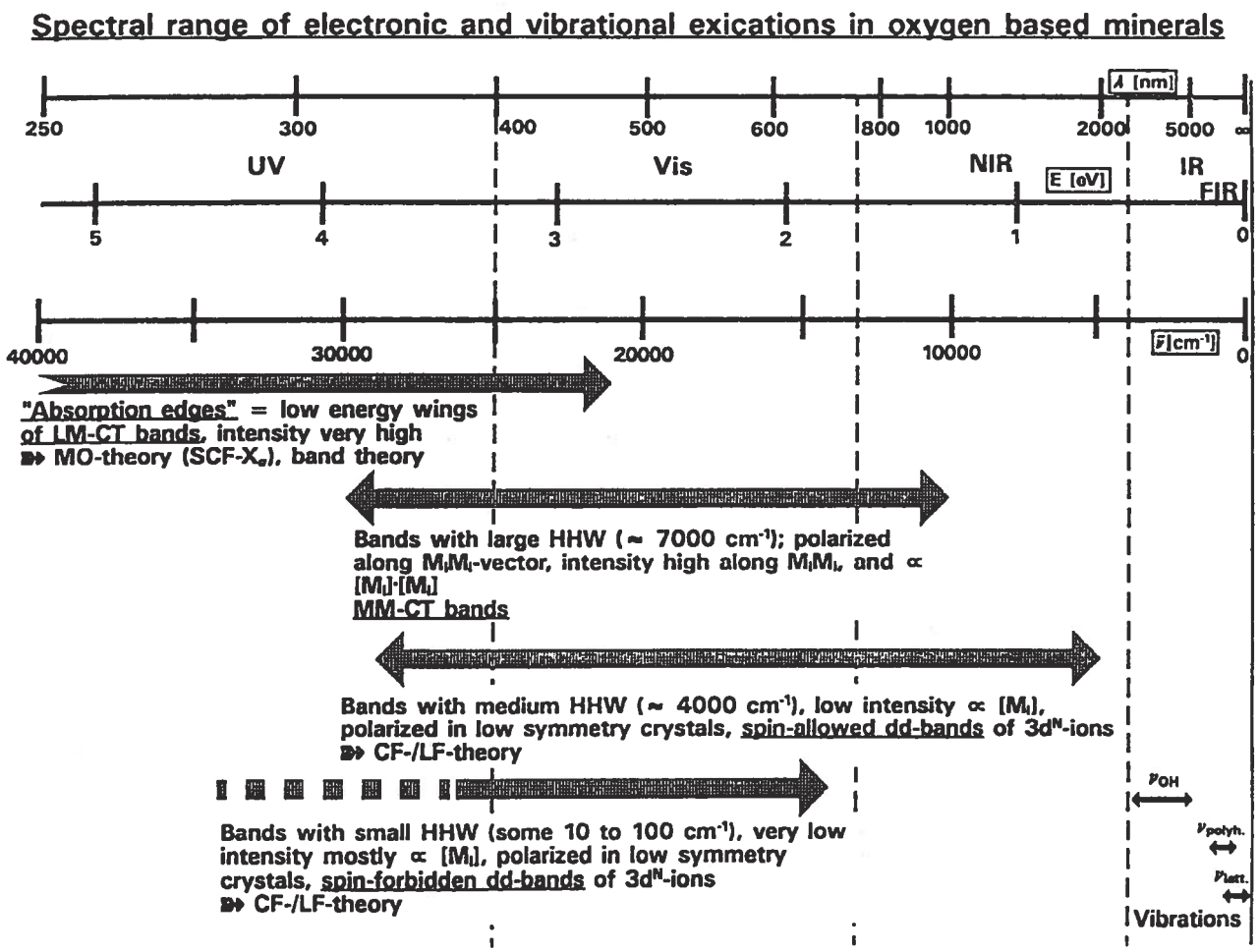

Fig. 1. Parts of the spectral range of electromagnetic radiation and energetic transitions excited therin in oxygen-based minerals. Some typical properties of the resulting absorption bands are also indicated. The abscissa is given in different scalings related to each other by transformation factors in the text. Note that the wavelength scale is distorted when compared to the related energy scales.

ber. The conversion factors are used to obtain the various scalings of the radiation energy in Fig. 1 while the relation between the wavelength on top of Fig. 1, and the wavenumber is given by the reciprocity between both these quantites. Fig. 1 shows that the wavelength scale is, due to this reciprocity, compressed at high wavelengths compared to the energy-scales. Therefore, absorption spectra should not be displayed in the wavelength-normal but in the energy-normal mode. Otherwise, the absorption bands caused by energy-related excitation processes will be distorted (expanded toward long wavelengths), an effect which is shown by all the wavelength-normal spectra presented in the otherwise very meritorious book of Burns (1993).

Excitation of electronic transitions from the energetic ground state to excited states with higher energies and related relaxation processes, $\Psi \leftrightarrow \Psi^*$, are quantized processes. Hence, they show up as "bands" in absorption spectra, *i. e.* in scans of the types

$$\left.\begin{array}{ll} \text{Transmission,} & T = I/I_o \\ \text{or Absorbance} & \\ \text{(sometimes called} & A = \lg(I_o/I) \\ \text{"optical density"),} & \\ \text{or Linear absorption} & \alpha_{[cm^{-1}]} = A/t \\ \text{coefficient,} & \end{array}\right\} = f\left\{\begin{array}{l} (\lambda_{[nm]}) \quad \text{or} \\ (E_{[cm^{-1}]} = 1/\lambda_{[cm]}) \quad \text{or} \\ E_{[eV]} \end{array}\right. \qquad (5)$$

Here, I_o and I are the intensities of incoming and outgoing light from the plane-parallel crystal plate under study, t is its thickness in cm. The absorbance A is defined on the basis of the exponential decrease of (1/T) on increasing t as given by Lambert's law.

The absorption bands in absorption spectra are characterized by the energy position E, *e. g.* in wavenumbers [cm^{-1}], of their intensity maximum, by the linear absorption coefficient α, in cm^{-1}, in the intensity maximum over the background and by the full band width at half height $\Delta v_{1/2\,B}$. In the case of anisotropic minerals which are lower in symmetry than cubic, α_{max} may depend on the orientation of the crystal with respect to the electric vector of the polarized radiation, causing polarization dependencies of band intensities, *i. e.* pleochroism. A further characteristic of absorption bands is that they may be modelled by relatively simple distribution functions, when the quantities to plot the spectra are chosen such that band distortions are avoided. Bands in electronic spectra can be represented by Gaussians (Jørgensen 1964) when an energy unit is chosen for the spectrum abscissa and A or α for the ordinate. However, the Gaussians may be mixed with Lorentzian components. This is important in the analysis of complex band envelopes.

1.2 Types of transitions causing absorption bands

Fig. 2 displays the schematically drawn spectra of chromium-rich uvarovite and chromium-poor pyrope to show the principal features in accord with the principles discussed above. What type of excitations give rise to the absorption bands and edges displayed? The lower part of Fig. 1 shows the energy ranges of excitations between the respective energetic ground state and the excited higher energetic states, $\Psi \rightarrow \Psi^*$. Below 4000 cm^{-1}, sharp vibrational bands of OH^- may occur (Fig. 2) caused by structural defects in the case of nominally "water"-free garnets (Matsyuk *et al.* 1998; also for the previous literature). The lattice vibrations show up as sharp and extremely intense bands the top of which may only be measured on ultrathin crystal platelets with t in the µm-range (Fig. 2). These absorption bands will not be discussed further, as this paper is concerned with electronic transitions. From Fig. 1, it may be seen that there are three types of these latter excitation mechanisms:

1. LM-CT: Electron charge-transfer between the oxygen

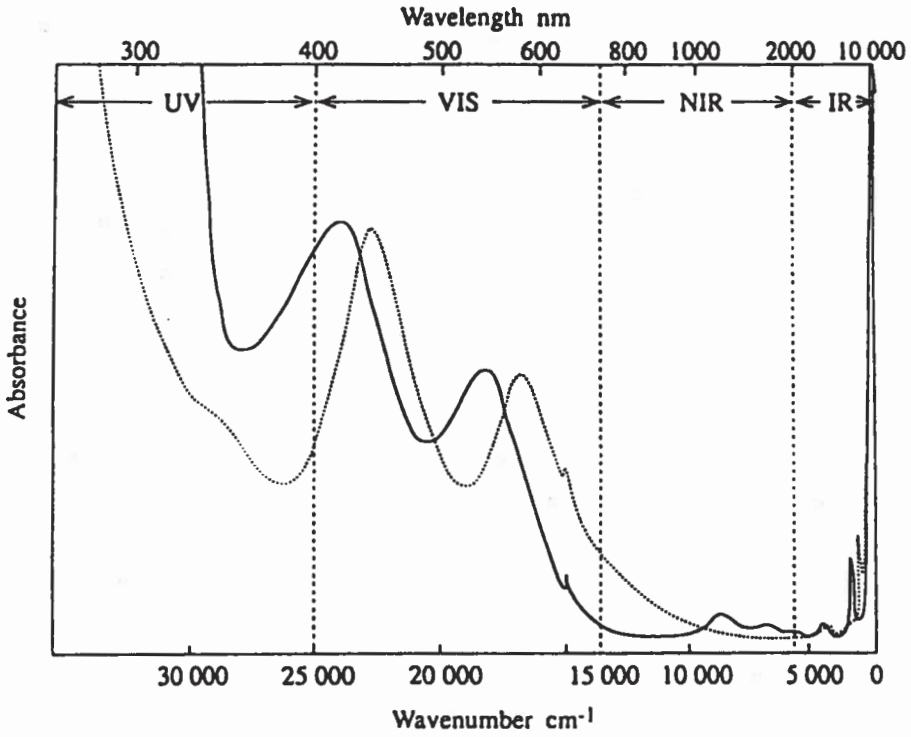

Fig. 2. The principal features of a typical abssorption spectrum in the UV/VIS/NIR range demonstrated schematically for two garnets, a pyrope with 5.5 wt % Cr_2O_3 (solid line) and a uvarovite with 17 wt % Cr_2O_3 (dotted line) (after Langer 1988).

ligands and central ions in the polyhedra of the respective crystal structure. In a strongly simplified scheme, LM-CT may be expressed as

$$[M^{(n+)} + O^{2-}]^{[CN]} \leftrightarrow [M^{(n-1)+} + O^{-}]^{[CN]} \quad (6)$$

The arrows → and ← indicate excitation and relaxation, respectively. Such LM-CT transitions give rise to extremely intense bands in the UV, the tops of which have so far not been measured in transmitted light. The low-energy wings of such bands form the so-called absorption edges ocurring in the low-energy UV, violet and blue (Figs 1 and 2). The energy position of the edges depend on the type and charge, as well as on the concentration of the ions $M^{(n+)}$ in the crystal, on the oxygen-metal distance R_{M-O}, and on the coordination number in the cluster. Here, only such LM-CT will shortly be discussed which involves transition-metal ions $M^{(n+)}$ as in such cases the transition with lowest energy occur below the vacuum-UV (<55500 cm^{-1}). From quantum mechanical calculations of the molecular orbitals of the respective clusters, it is obvious that the lowest-energy LM-CT transitions decrease in the order

$$(Mn^{2+}O_6)^{10-} > (Cr^{3+}O_6)^{9-} > (Ti^{3+}O_6)^{9-} > (Fe^{2+}O_6)^{10-} > (Ti^{4+}O_6)^{8-} > (Fe^{3+}O_6)^{9-} \quad (7)$$

in their energies, the range extending from 56500 cm^{-1} for Mn^{2+} to 25300 cm^{-1} for Fe^{3+} (Tossell *et al.* 1974, Löffler *et al.* 1974, Sherman 1984). Eqn. (7) shows that in case of constant atomic number but increasing valence of M, the energy of LM-CT decreases. This is also obvious from

$$(Mn^{2+}O_6)^{10-} > (Mn^{3+}O_6)^{9-} > (Mn^{4-}O_6)^{8-} \quad (8)$$

with energies between 56500 and 34800 cm^{-1} (Sherman 1984). Decreasing ligand-to-metal distance, $R_{M^{(n+)}-O}$ (*e. g.* in $(Fe^{2+}O_6)^{10-}$ octahedra) enhances the energy of the lowest LM-CT transition according to calculation (Tossell 1976), which is at variance with experimental results on the p-dependence of the absorption edge (*e. g.* Mao 1976, Burns 1982, Smith – Langer 1982a). Coordination number and type of ligands also have an important influence on the energy of the lowest LM-CT transition as obvious from the sequence

$$(Fe^{2+}O_6)^{10-}_{37500} > (Fe^{2+}O_4)^{6-}_{29150} > (Fe^{2+}S_4)^{6-}_{14500} \quad (9)$$

where the calculated energies (Löffler *et al.* 1974, Tossell *et al.* 1974, Vaughan *et al.* 1974) are given as subscripts. In the case of sulfur ligands of tetrahedrally coordinated iron, the LM-CT energy is situated in the NIR (*cf.* spectral ranges in Fig. 1). This is the reason for the opaque appearance of Fe-bearing sphalerite.

In the case of the garnet spectra of Fig. 2, the steep increase of absorbance in the UV is caused by excitation of LM-CT, the energy of the edge in the case of pyrope occurring at lower energy than that of uvarovite due to the presence of some $Fe^{2+[8]}$ in the former mineral (*cf.* eqn. (7)).

2. MM-CT: Electron charge-transfer between transition-metal ions different in charge and allocated in neigbouring structural polyhedra which are interconnected by a common edge or face. Such excitations may be represented in the following strongly simplifying scheme

$$M_1^{(n+)}\,[\text{polyh. 1}] + M_2^{(m+)}\,[\text{polyh. 2}] \leftrightarrow M_1^{(n-1)+}\,\{\text{polyh. 1}] + M_2^{(m+1)+}\{\text{polyh. 2}] \quad (10)$$

Absorption bands caused by excitation of MM-CT may occur in the visible and neighbouring spectral ranges (Fig. 1), depending on the type of the two exchanging transition-metal ions M_1 and M_2, their distance from each other, R_{M1M2}, in the structure (Smith – Strens 1976), the types of the polyhedra 1 and 2 and their connecting geometrical element, common edge or face, as well as the O-O distance involved (Khomenko *et al.* 1986, Khomenko – Platonov 1996). Also the extension of the interconnected units in the structure (pairs, chains, walls) have an influence on the energy of MM-CT (Amthauer – Rossman 1984). Generally, homonuclear MM-CT (*e. g.* $Fe^{2+}Fe^{3+}$-CT) occurs at lower energies than heteronuclear MM-CT (*e. g.* $Fe^{2+}Ti^{4+}$-CT). In both cases, the excitation energies decrease with decreasing distance R_{M1M2}, with increasing cluster size, and in the sequence edge connection – face connection. As often verified, the most characteristic property of bands caused by MM-CT is a strict polarization along the MM-vector in the respective crystal structure (*cf.* Platonov *et al.* 2000, also for older literature). Mattson – Rossman (1987) found that large band width, in the order of 5000 to 6000 cm^{-1}, is the most reliable characteristic of MM-CT. Smith and Strens (1976) showed that band intensity is related to the concentration product, $[M_1]*[M_2]$, rather than to the concentration of one specific transition-metal ion.

Sherman (1987a, b) calculated the molecular-orbital diagrams for clusters of two edge-connected octahedra with the homonuclear or heteronuclear compositions $(FeFeO_{10})^{14-}$ and $(FeTiO_{10})^{14-}$ and with central-ion distances R_{M1M2} of 2.94 and 2.91 Å, respectively. The results were energies for the optical excitation of $Fe^{[6]}Fe^{[6]}$-CT as 10570 cm^{-1} (at $q = \lambda$, *cf.* Sherman 1987a) and of $Fe^{[6]}Ti^{[6]}$-CT as 18040 cm^{-1} (Sherman 1987b). Such values are somewhat lower than those typically found in the respective mineral spectra at around 13000 cm^{-1} or around 21000 cm^{-1}.

MM-CT is excited in a large number of oxygen-based minerals as iron in both valencies as well as titanium are so abundant, at least in trace amounts. Excitation of MM-CT causes typically deep-blue colour as in kyanite and glaucophane or a nearly opaque appearance as of biotite or iron-rich chlorites. The introductory garnet spectra of Fig. 2 do not show bands with the characteristic properties of MM-CT.

(3) dd-transitions: Electrons in the incompletely filled d-states of the $3d^N$-transition metal ions (or d- and/or f-states of transition metal ions of higher periods in the periodic table of the elements) may undergo the so-called spin-allowed, sa-dd, or spinforbidden transitions, sf-dd, when such ions are incorporated in the crystal-field made up by a non-sperical arrangement of negatively charged ligands forming the respctive coordination polyhedra with coordination number [CN] and the respective site symmetry in the crystal structure. In such a case, the five 3d-orbitals which are energetically and symmetrically equivalent – degenerate – in a spherical field of the same strength, are crystal-field split. Such crystal-field splitting opens the possibility of transitions between these now energetically and symmetrically different split states. However the dd-transitions that would result, are forbidden by quantum-mechanical selection rules.

The Laporte rule implies that transitions cannot occur when Ψ and Ψ^* would have the same sign, which is the case for all dd-ransitions. This selection rule can at least

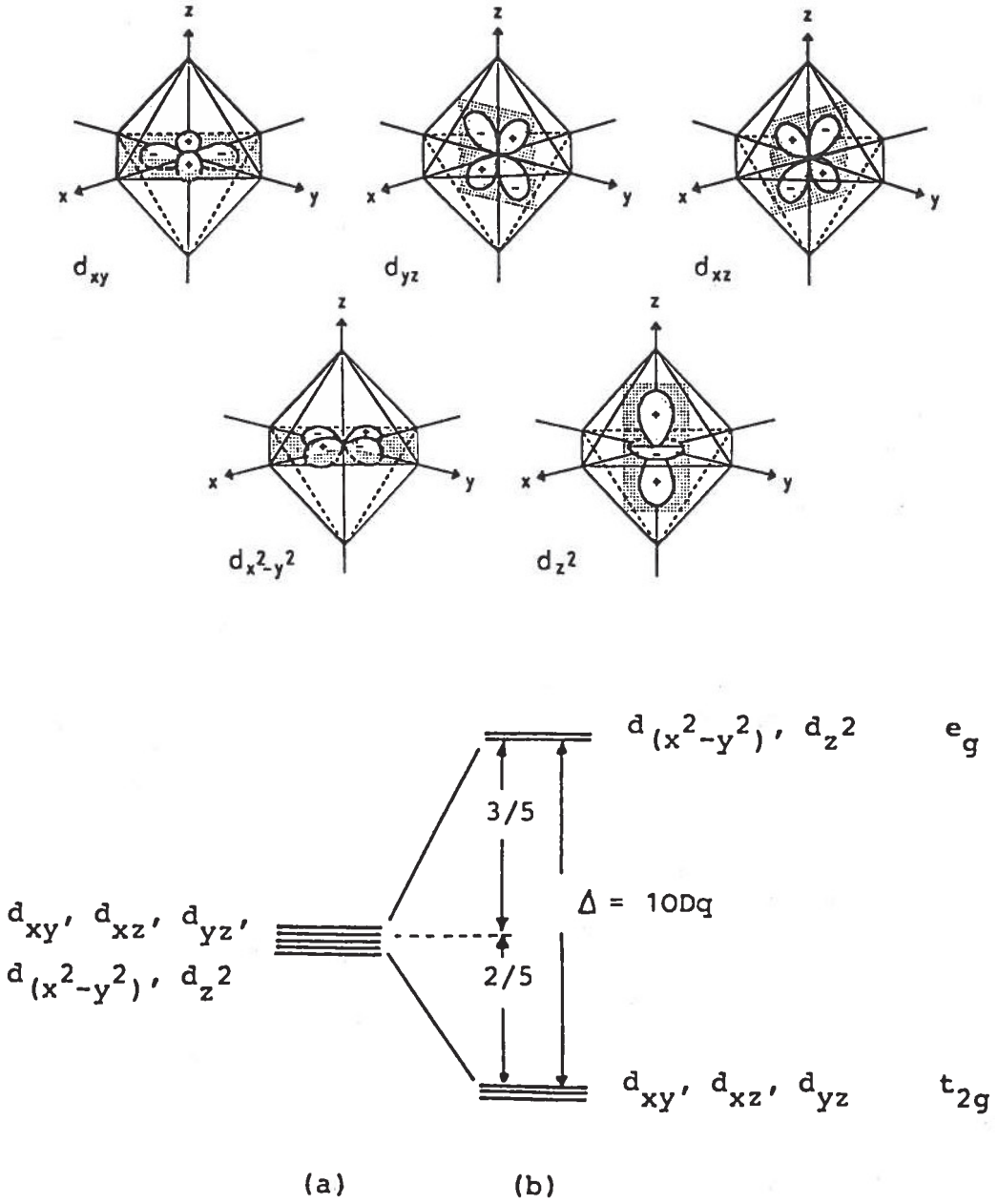

Fig. 3. Graphical representation of the solutions of the wavefunctions with d-character, the d-orbitals of $3d^N$-ions. These are shown in an octahedral field of negatively charged ligands to explain the energy splitting caused by a non-spherical electrical field of point symmetry O_h. The Figure's lower part shows the crystal field splitting for N = 1, the one-electron case: The d-states are energetically and symmetrically the same, *i. e.* fully degenate in a spherical field (a) of an otherwise undisturbed free ion. In the case of a non-spherical octahedral field the degeneracy is partly lifted (b). This is called crystal field splitting.

in part be overcome by dynamic or static lifting of any center of symmetry occurring at the $3d^N$-site in the respective crystal structure. By this, the spin-allowed dd-transitions, dd-sa, become active, though their intensity (related to the transition probability) is usually much lower than that of the bands caused by LM-CT or MM-CT, in the latter case along the MM-vector. The spin-selection rule forbids transitions in which, simply speaking, energy and symmetry of a d-electron and – at the same time – the direction of its spin-momentum, + or –, is changed. Nevertheless, such transitions may occur, the spin-forbidden dd-transitions, dd-sf. Due to the two selection rules, they may show up in electronic spectra with very weak intensity and with very small half widths, as they are activated by the above-mentiond effects and by coupling effects not discussed here.

Fig. 3 shows, in the upper part, the 3d-orbitals which are degenerate in the case of a spherical field, as shown in the Fig.'s lower part, left. As obvious from the orientation of the orbitals and the positions of the six negatively charged oxygen ligands in an octahedron with point symmetry O_h, shown in the upper part of Fig. 3, the orbitals become energetically and symmetrically inequivalent (Fig. 3). They split into two sets, the simply degenerate e_g-states, with enhanced energy compared to the spherical case, and the triply degenerate t_{2g}-states, with lowered energy compared to the spherical case. The total crystal-field splitting in an octahedral field with point symmetry O_h is characterized by the crystal-field parameter Δ_o. The splitting scheme in the lower part of Fig. 3 suggests the possibility of dd-sa transitions of the type $t_{2g} \rightarrow e_g$. In tetrahedral fields, point group T_d, and cubal fields, point group O_h, the sequence of the crystal-field terms is reversed. The respective crystal-field parameters are related by

$$\Delta_{oct} : \Delta_{cub} : \Delta_{tetr} = 1 : (-8/9) : (-4/9) \qquad (11)$$

(Burns 1993). Note that the crystal-field diagram in the lower part of Fig. 3 is valid for the configuration d^1 only. Nevertheless, it is widespread practice to use this one-electron scheme also for d^N-multielectron cases by filling in the N d-electrons in accord with the Pauli-principle (*cf.* Burns 1993). Correct is the description of d^N-multielectron cases by using the symbols for the irreducible representations of the symmetries of the respective electron distributions, to characterize the energy levels of the $3d^N$-ion in the respective crystal-field (*cf. e. g.* Marfunin 1977). The upper part of Fig. 4 illustrates the relations between the one-electron model and the correct representation for the case of the crystal-field splitting of the spectroscopic ground state ^4F of the $3d^3$-configurated Cr^{3+} in spherical field. In an octahedral field, point group O_h, there result three crystal-field states, $^4A_{2g}$, $^4T_{2g}$ and $^4T_{1g}$ from crystal-field splitting of the totally degenerate ^4F ground state of the spherical Cr^{3+}. Such splitting enables then two dd-sa transitions, $^4A_{2g} \rightarrow {}^4T_{2g}$ and $^4A_{2g} \rightarrow {}^4T_{1g}$, as obvious from the right side of the upper part of Fig. 4. These transitions are also symbolized in the one-electron model on the left side. The middle part of Fig. 4 shows the octahedral crystal-field splitting of the fully degenerate spectroscopic ground states of all the $3d^N$-ions in octahedral fields of point group O_h. From this, four important aspects of dd-transitions become obvious:

(i) As far as splitting of spectroscopic ground states is concerned, we can expect one dd-sa transition in the case of the $3d^N$-ions with N = 1, 4, 6 and 9, two such transitions in case of N = 2, 3, 7 and 8 and none in the ions with N = 5, Mn^{2+} and Fe^{3+}, as their free ion ground state ^6S does not split. The schematic spectra of the garnets (Fig. 2) show the two dd-sa transitions expected for Cr^{3+}[6], as relatively strong bands with half widths near 3500 cm^{-1}. Typical dd-sf bands of Cr^{3+} are schematically shown in Fig. 2 near 14500 cm^{-1}, with their characteristic very low intensity and very small band width.

(ii) The crystal-field ground states of the $3d^N$-ions with N = 1, 2, 4 6. 7 and 9 and the excited states of all the $3d^N$-ions, except for the uppermost states in case of N =2 and 7 are degenerate E or triply degenerate T in octahedral fields with point group O_h. These degeneracies are lifted in crystal fields of six oxygen ligands arranged such that octahedral coordination is resembled but the symmetry is reduced from regular, *i. e.* in distorted "octahedra", as they normally occur in mineral structures. Such lifting of degeneracies of the crystal-field states result in more transitions than the above mentioned ones. As a consequence, band splittings may occur in distorted, low-symmetry "octahedra". In such cases, symmetry-selection rules allow the respective transitions along certain internal directions only, in the low-symmetry "octahedra" (*cf. e. g.* Rossman 1988, Langer 1988). This causes the intensities of component bands, resulting from low-symmetry band splittings, to be polarized, the explanation of pleochroism. To reverse this reasoning, the point symmetry of the involved "octahedra" may be determined by analysing the band polarizations (*cf. e. g.* Marfunin 1979). In most such procedures, when successful, point groups higher in symmetry than the site symmetries of the involved crystallographic sites are obtained, so-called pseudo-symmetries.

(iii) The bands caused by dd-sa transitions between states, derived from crystal-field splitting of the totally degenerate spectroscopic ground states of the $3d^N$-ions, as presented in the middle part of Fig. 4 or between states produced from these by low-symmetry splitting are specific for each $3d^N$-ion. This is obvious from Fig. 4 and the discussion of point (ii), as well as from the fact that the crystal-field parameters 10Dq of the $3d^N$-ions are specific for a specific N, when we neglect for a moment variations of 10Dq (to be outlined next). The 10Dq-values of some $3d^N$-ions in aqueous solutions are (Burns 1993):

N	1	2	3	4	5[1]	6	7	8	9	(12)
Ti^{3+}	V^{3+}	Cr^{3+}	Mn^{3+}	Mn^{2+}	Fe^{3+}	Fe^{2+}	Co^{2+}	Ni^{2+}	Cu^{2+}	
18950	19100	17400	21000	7800	13700	9400	9300	8500	3000	cm^{-1}

[1] 10Dq-values of the d^5-ions are extracted from dd-sf transitions

The octahedral crystal-field parameter of each specific $3d^N$-ion depends on the type of ligands, on their effective charge, $(Z_L \cdot e^2)$, and the mean distance between cation and ligands. Here, we concentrate on O^{2-}- ligands in oxygen-based minerals and may, therfore, neglect the influence of different covalencies of the ligand-metal

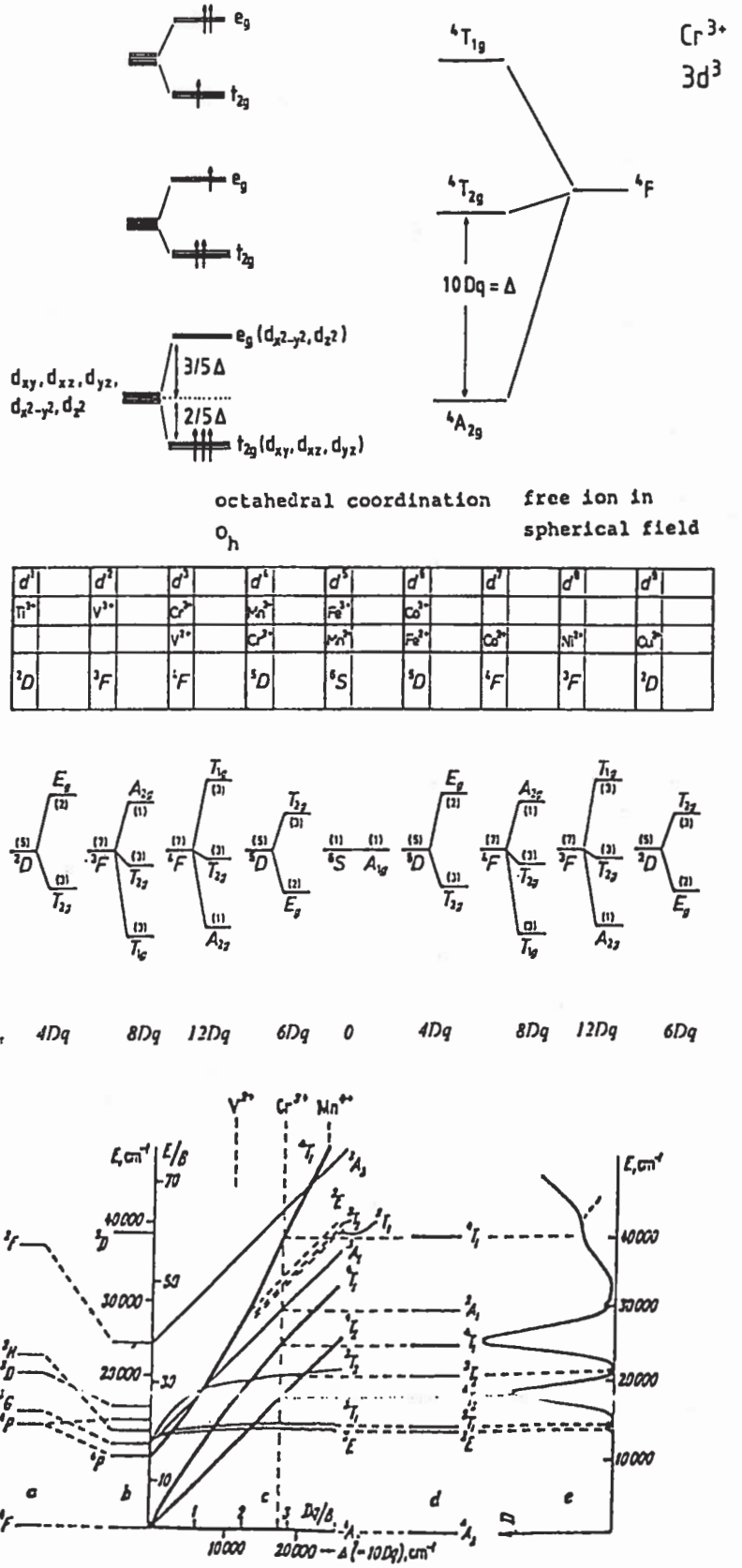

Fig. 4. Crystal field splitting and electronic transitions in $3d^1$, or $3d^N$-or multi-electron cases. Upper part: Electronic states for the example N = 3, left in the one-electron model and right in the correct notation of multi-electron cases by means of the symbols for the irreducible representations of the respective symmetries of the electron distributions. Middle part: Octahedral crystal field splittings of the totally degenerate spectroscopic ground states for all the $3d^N$-ions and their crystal field stabilization energies in terms of Dq, where 10Dq = octahedral crystal field splitting parameter. Lower part: Crystal field splitting of the spectroscopic ground state and the excited spectroscopic free ion states (spherical field) of a $3d^N$-ion for the examples of N = 3 and dependence of the resulting crystal field states on its strength 10Dq, *i. e.* a Tanabe-Sugano diagram. In such diagrams, 10Dq-values are normalized in terms Racah-parameter B (see text). Also, the diagrams are normalized such that the ground state has always E = 0.

bonds produced by other ligands, in accord with the nephelauxetic series (*cf.* Burns 1993). 10Dq of a specific $3d^N$-ion, such that the radial distance of the d-orbitals, r, can be regarded as constant, is given by the relation

$$10Dq_{3d^N} = (5/3) \cdot (Z_L \cdot e^2) \cdot \langle r^4 \rangle \cdot R^{-5} \qquad (13)$$

This relation (derived from crystal-field theory, Dunn *et al.* 1965) is shown to be valid over a large range of R by recent quantum-mechanical ab-initio calculations of fayalite spectra (Krasovska *et al.* 1997). The characters and field dependencies of the energies of crystal-field split terms of all spectroscopic states of all the $3d^N$ transition metal ions in octahedral coordination O_h, were quantum mechanically calculated by Tanabe – Sugano (1954a, b). As an example, the Tanabe – Sugano diagram for N = 3, *i. e.* for Cr^{3+}, is shown in the lower part of Fig. 4. In such diagrams, 10Dq as well as the energy E, are normalized with respect to B, such that the diagram applies for different ions with the same N, here V^{2+}, Cr^{3+} and Mn^{4+}. B is one of the Racah parameters introduced in the quantum-mechanical calculations, to account for repulsion of the N d-electrons. This repulsion decreases on incorporation of the respective $3d^N$-ion in the nonsperical crystal fields and decreases further on increasing covalency of the M-O bond in the $3d^N$-ion centered polyhedra. Hence, the so-called nephelauxetic ratio

$$\beta = B_{field}^{3d^N} / B_{free}^{3d^N} \qquad (14)$$

is a relative measure of covalency. The necessary free-ion B-values are also given by Tanabe and Sugano (1954a, b).

(iv) From the splitting schemes in Fig. 4, it is obvious that the ground-state energies of the $3d^N$-ions in the non-spherical crystal field are lowered compared to the ground states in spherical field. These losses in energy stabilize the $3d^N$-ions in non-spherical fields. The amounts of such crystal-field stabilization energies, CFSE, in multiples of Dq, are included in the middle part of Fig. 4 for the case of octahedral coordination. For other regular coordinations, these may be recalculated by eqn. (11). When the ground states are degenerate in regular coordinations as discussed under point (ii), then ground-state splitting will result in low-symmetry fields, which adds to the CFSE obtained from 10Dq in the respective regular octahedral site. Crystal-field stabilization may play an important role in the thermodynamics of $3d^N$-ion bearing minerals, as will be shown below for intercrystalline partioning of Cr^{3+} (Langer – Andrut 1996) and Fe^{2+} (Langer – Khomenko 1999).

To finish this theoretical introduction, it is to be added that values of 10Dq and B can be extracted from electronic absorption-spectra on the basis of the results of quantum-mechanical calculations by Tanabe – Sugano (1954a, b; the solutions for the energy difference between the states are found *e. g.* in Langer 1988).

1.3 Information to be extracted from electronic absorption-spectra of single crystals of oxygen-based minerals

The theoretical aspects introduced in the foregoing, are essential to understand that much information, valuable in structural research and in those parts of geosciences which are concerned with the physics and physico-chemistry of oxygen-based minerals, can be extracted from polarized single-crystal absorption spectra in the range of electronic excitations. Table 1 is an overview on the information that may be obtained, and needs only one, though important, comment:

The extraction, from electronic spectra, of the data listed in Table 1 is only possible when the assignments of the observed bands to the causal excitations are correct. This presupposition may be difficult to achieve in the case of chemically complex minerals in which a variety of different excitation mechanisms and/or, of dd-transitions of different $3d^N$-ions eventually present in the respective mineral crystal, give rise to complex spectral envelopes of overlapping sets of bands. These difficulties can eventually be overcome by

(A) Reliable band assignment of spectra measured on chemically simple minerals, before analyzing the spectra of chemically more complex ones with the same structure type. "Chemically simple" means with a composition that allows for one type of excitation only. Mineral-crystals serving this purpose have to be carefully selected.

(B) It is possible to achieve (A) using synthetic minerals, crystals of which are grown under carefully controlled physicochemical conditions of p_{total}, f_{O2} and eventually other fugacities of fluid components, T and bulk composition X, such that only one type of excitation mechanism can be present in the synthetic crystals. This approach (Langer – Abu-Eid 1977) has often been used sucessfully by the author and coworkers (as shown in the results section). Because the synthetic crystals are often too small to measure in conventional spectrometers, microscope-spectrometric methods are essential in this approach (B).

(C) The solution of the problem may also be approached by studying a set of natural crystals with different concentrations of the different $3d^N$-ions allocated in the respective mineral and check for dependencies of band intensities on ion concentrations. This approach was successfully used by Moore – White (1972) to assign dd-sf transitions in garnets.

(D) Excitations of the different types show often characteristic positions or ranges of band energy. They show also characteristic band widths as well as characteristic concentration dependencies and polarizations of their band intensities.

(E) Energies, widths and intensities of bands caused by the excitation of LM-CT, MM-CT and dd-sa with or without inversion centre at the $3d^N$-ion site, or dd-sf exhibit characteristic p, T dependencies (Abu-Eid 1976, Abu-Eid – Burns 1976, Burns 1982). These results were

Table 1. Which information on the structure, physics, chemistry and physico-chemistry of oxygen-based minerals can be extracted from their polarized single crystal absorption spectra in the UV to NIR spectra ranges?

A. Information, to be gathered independent on an assignement of the absorption bands in the spectra measured

A.1 Phenomenological interpretation of colour and pleochroism, quantification by means of proper parameters and the quantization of spectra by their use to obtain colour charts
A.2 Determination of radiative heat transfer through "optical windows" and their p,T-dependence, including anisotropy effects

B. Information to be gathered from spectra wherein correct band assignements were achieved

LM-CT transitions:

B.1 Band gaps, electronic conductivity
B.2 Structure defects

MM-CT-transitions:

B.3 Intracrystalline distribution of the cations involved in the excitation of MM-CT

dd-transitions of $3d^N$-ions:

B.4 Type of ion/ions giving rise to the bands, including valency
B.5 Concentration of the respective ion/ions in the mineral studied
B.6 Concentration of the respective ion/ions in its/their specific structural site/sites in a multi-site structure (site fractions)
B.7 Kinetics of intracrystalline distribution reactions
B.8 (Pseudo-) Symmetry of the $3d^N$-ion centered sites - by evaluation of 10Dq and its p- and T-dependence:
B.9 Mean local polyhedral distances in $3d^N$-ion bearing solid solutions
B.10 Local polyhedral compressibility
B.11 Local polyhedral thermal expansion
B.12 Crystal field stabilization energy, $CFSE_{3d}N$, and its influence on intra- and intercrystalline $3d^N$-ion distribution and on the thermodynamics of solid solotions - by evaluation of B and its p- and T-dendence:
B.13 Relative ionicity of the $3d^N$-ion - ligand bond, and p- or T-induced changes in it, influences of next-next neighbours

recently checked, proven or disproven, and further extended (Taran *et al.* 1994, 1996, Langer *et al.* 1996, Taran – Langer 1998, 2000). Such p, T-dependencies of band properties, different for different excitation mechanisms may also help to solve assignment problems.

2. Microscope-spectrometric methods

To the author's knowledge, Corin (1931) was the first to conceive and use microscope-spectrometric methods, though in a part of the visible spectrum only and with relatively large measuring spots (Fig. 5). This author used a spectroscope in a microscope's tubing and photographic registration. A similar spectroscopic apparatus, but recording the transmitted radiation by means of a photo-multiplier, was designed and used by Grum-Grzhimailo (1953). Further development led to instruments to which a wider spectral range and smaller measuring spots are available (Fig. 5). The difficulty to adjust two microscopes in measuring or reference beams, respectively, of high-resolution spectrometers (Burns 1966, Mao – Bell 1971) was overcome by single-beam methods which use the wavenumber step-scanning procedure (Platonov 1976, Langer – Abu-Eid 1977, Langer – Frentup 1979).

A scheme of the automated version of such an instrument allowing for measurements in the wide spectral range 40000 to 5000 cm^{-1} on spots with effective diameters down to about 5 mm in such spectral ranges where the beam intensity and detector sensitivity are high (Langer – Frentrup 1979), is shown in Fig. 6. The instrument is based on a Zeiss research microscope equipped with UV-transmittant objectives 10x, 32x and 100x and UV condenser (Zeiss ULTRAFLUAR), which are chromatically completely corrected in the range 50000 to 12000 cm^{-1} and a Glan-Thompson type calcite polarizer effective to over 95 % in the same spectral range. A double-prism SiO-glass monochromator and a photometer head are attached to the instrument. The scheme of Fig. 6 shows that an image of the prisms is produced in the plane of the entrance diaphragm, in the object plane, and in the plane of the exit diaphragm. Hence, the absolute diameter of the entrance diagphragm, together with the magnification of the condenser, define the effective diameter, d_a, of the illuminated area in the object plane. The smallest d_a may be about 8 μm. Furthermore, in the divergent beam produced by the objective a smaller measuring area with diameter, d_m, may be cut from the image of the illuminated area by setting exit diaphragms with appropriate absolute diameter and using objectives with appropriate magnification. Smallest d_m may be about 3 μm in favourable spectral ranges. The sensitivity of the whole setup using either an RCA IP-28 or an RCA C-31025 C multiplier, UV-transparent objective 100x with 40 % transmittance at 40000 cm^{-1} and with measuring apertures down to 4 μm was checked by measuring in the beginning of our microscope-spectrometric studies (Langer – Abu-Eid 1977) and also with an attached DAC (Smith – Langer 1982b) .

The spectral resolution depends on the spectral band width, $\Delta\bar{\nu}_{1/2M}$, of the measuring radiation. To obtain sufficient measuring intensity, $\Delta\bar{\nu}_{1/2M}$, cannot be smaller than 50 cm^{-1}. Thus all bands with $\Delta\bar{\nu}_{1/2B} \geq 500$ cm^{-1} are not subject to slit errors larger than 1 % (Ramsey 1952). Only some dd-sf transitions have $\Delta\bar{\nu}_{1/2B}$ below 200 cm^{-1} in minerals.

A problem may arise in microscope-spectrometry when the measuring radiation is strongly con- and divergent, as is the case when high magnification is used to measure polarized spectra. In such a case, the tops of strongly polarized bands will be truncated, an effect that results from mixing of polarizations of the non-parallel radiation inside the crystal (Goldman – Rossman 1977). However, in case of the ULTRAFLUAR 10x with numerical aperture 0.20, the convergance in air has an angle $\theta = 11.5°$ under which the effect will not exceed 3 % (Goldman – Rossman 1977). In any case, higher magni-

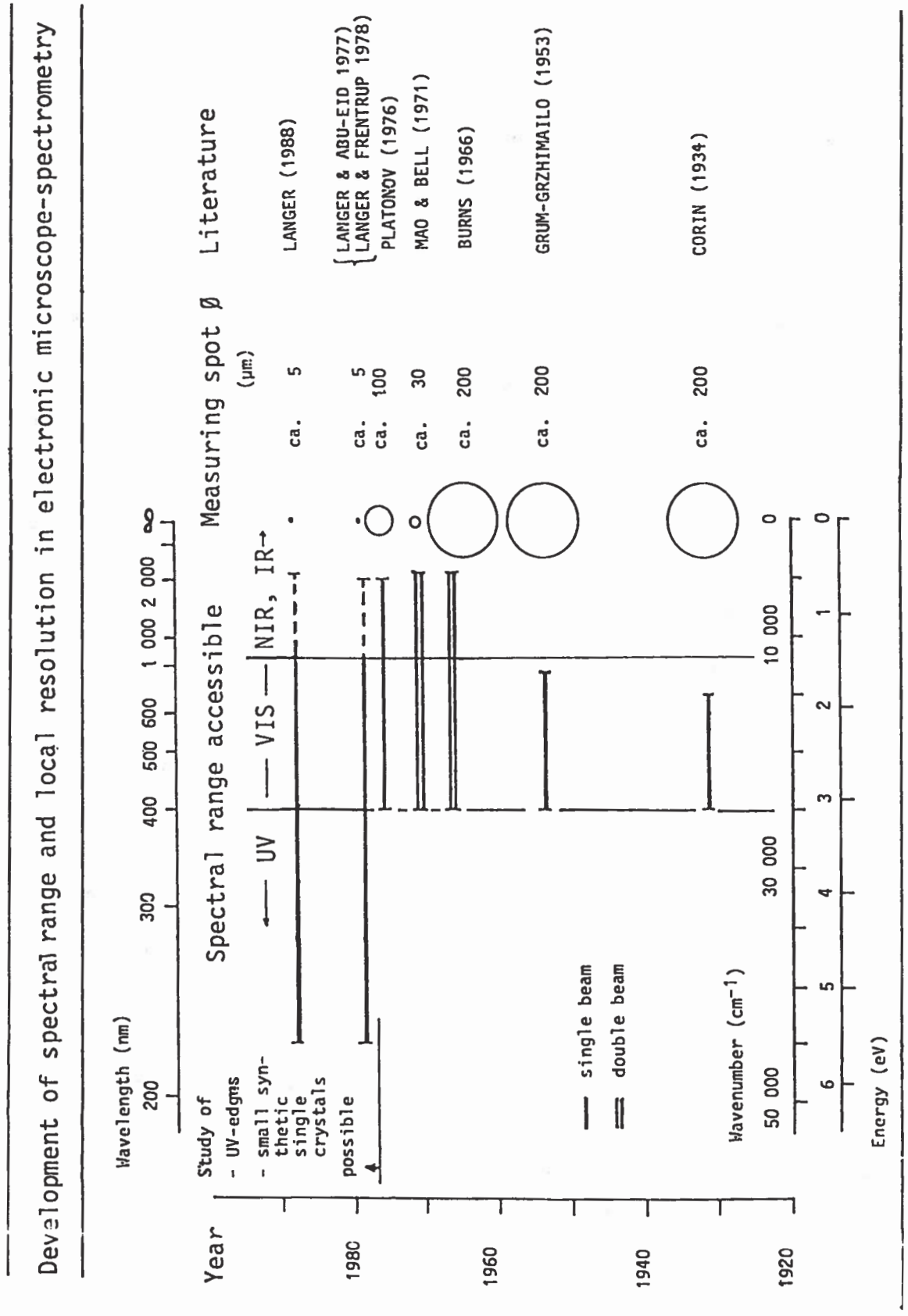

Fig. 5. Development with time of spectral ranges and areal resolution accessible to electronic microscope-spectrometry since its first conception by Corin (1934).

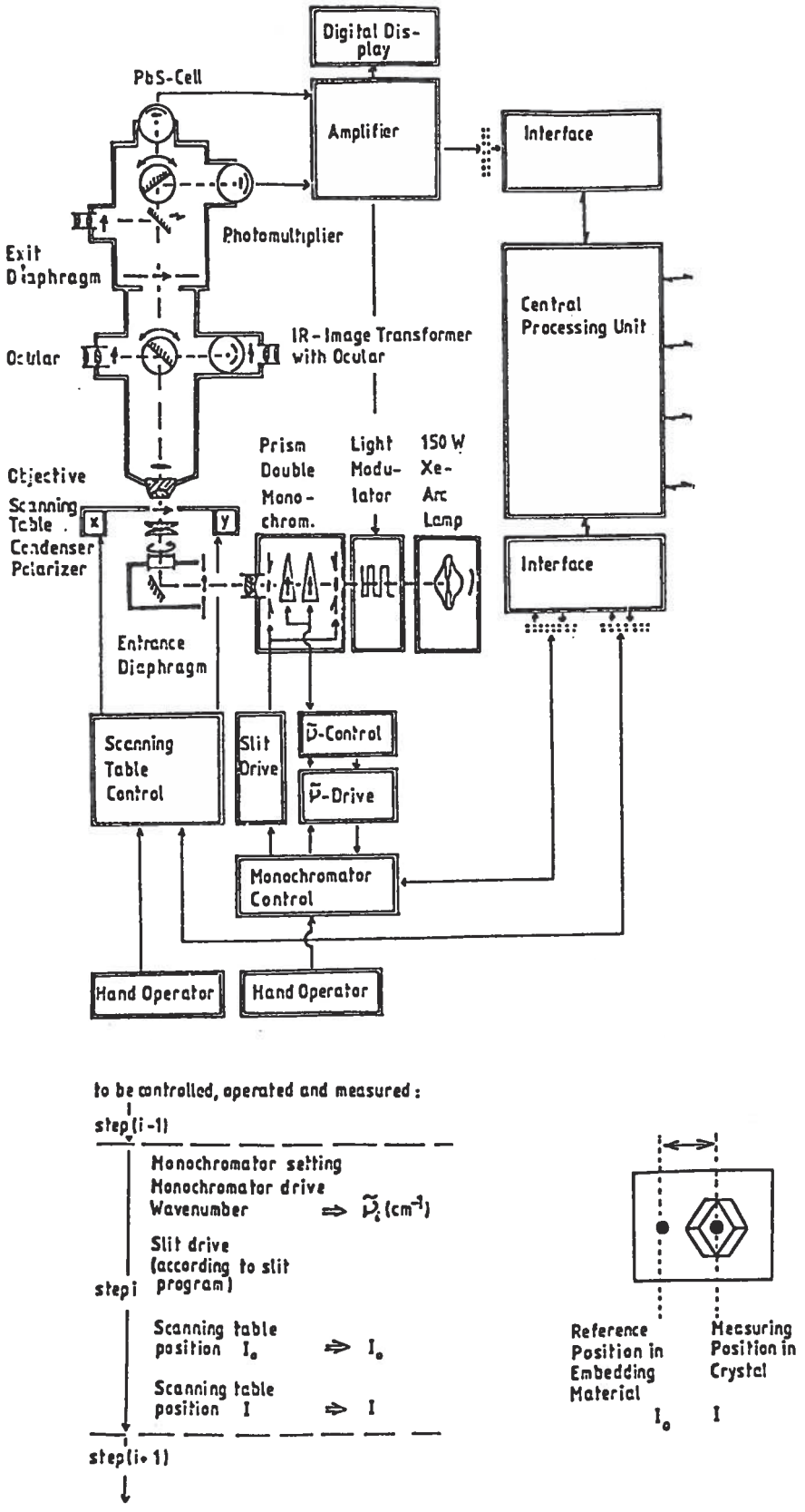

Fig. 6. Scheme of a microscope-spectrometer and of the wavenumber step scanning procedure in which it is operated (Langer – Frentrup 1979). Symbols: hardware, light path, control and measuring signals, monochromator slits, mirrors, images of arc or slits, images of prisms or object.

fications need careful consideration of possible errors caused by non-parallel measuring radiation.

Another limitation shows up when measuring very small crystals in the low-energy range and when these crystals have higher refractive index than the embedding material, as is usually the case. Then, diffraction effects at the grain boundary cause interference fringes which may overlap to produce crystal rims lighter than the outer embedding material where the I_o-reference measurements are taken, *i. e.* the Becke line. Fig. 7 shows examples (Langer – Abu-Eid 1977) representing scans of the Becke's diffraction phenomenon. The result in a spectrum of a very small crystal is that any band centered at low energy will show its low-energy wing falling below zero absorbance or will be totally suppressed.

The wavenumber step-scanning procedure of measurement is schematically illustrated by the small inserts at the bottom of Fig. 6. This type of measurement has the advantage of a high relative accuracy of absorbance measurements. In our laboratory, we are now using a Zeiss UMSP 80 which uses the continous scanning mode: First $I_o(\lambda)$ then $I(\lambda)$ is scanned, with recalculation to obtain log $(I_o/I)_\lambda = f(\bar{\nu})$. Also, the instrument is equipped with a grating monochromator with the avantage of λ- or $\bar{\nu}$-independent dispersion but with the disadvantage that the spectral resolutions to be achieved are not so high.

Spectra may be measured in a temperature range 77–873 K using a Linkam cooling-/heating-stage THM 600 using a silica window at low temperature and platini-

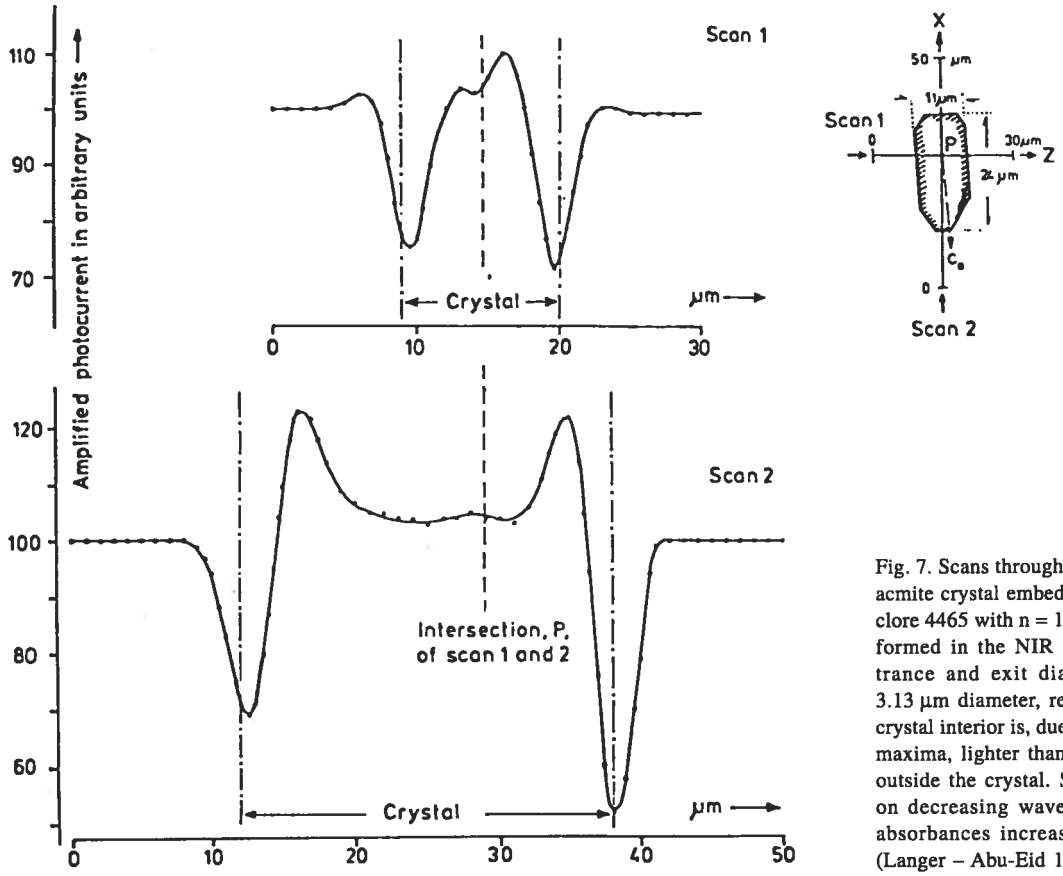

Fig. 7. Scans through the Becke-line of a small acmite crystal embedded in thermoplastic aroclore 4465 with n = 1.663. The scans were performed in the NIR at 10500 cm^{-1} using entrance and exit diaphramgms with 8 and 3.13 μm diameter, respectively. Note that the crystal interior is, due to unresolved diffraction maxima, lighter than the embedding material outside the crystal. Such effects are growing on decreasing wavenumber thus producing absorbances increasingly lower than 0.000 (Langer – Abu-Eid 1977).

num-wire grid as sample support at high temperature. High pressure single-crystal spectra are measured up to 200 kbar in a special diamond-anvil cell, designed such that the ULTRAFLUAR objectives with their relatively short working distances may dip into the pistons and that the tangential stress component on the pistons is as low as possible (Smith – Langer 1982b).

The preparation of non-regular crystals for measuring polarized spectra with the electrical vector E of the measuring radiation parallel to the main optical directions $X(n_o)$ and $Z(n_e)$ or $X(n_\alpha)$, $Y(n_\beta)$ and $Z(n_\gamma)$ requires careful work. Two methods are used:

(i) In case of crystals with longest dimension below 100 μm which cannot easily be handled as individual grains, powder mounts in glycerine are prepared on silica-glass carriers. Crystals, properly oriented for the just mentioned polarized measurements are looked for in the mounts. The disadvantage of this method is that crystal thicknesses cannot be measured and that optical misorientations may exceed some 5°. On the other hand, very small crystals with dimensions down to about 20 μm are accessible to measurement which can be carried on up to 40000 cm^{-1}, as glycerine does not absorb up to this wavenumber.

(ii) In case of crystals with longest dimension above 100 μm such that the grains can be handled individually, single-crystal mounts are prepared by orienting the crystals by X-ray diffraction or optical examination, embedding them oriented in a suitable resin on a glass carrier, and grinding and polishing them from both sides. A diaspore (010)-platelet or a quartz-platelet ∥ (0001) is also embedded aside the crystal for thickness measurment of the mount using the platelet's birefringence (*cf.* Čemić *et al.* 1986). This type of preparation has the disadvantage that resins available for embedding allow for measurements up to 33000 cm^{-1} only, due to their UV-absorption (Langer – Abu-Eid 1977). The advantage is that the orientation of the crystal is fixed to within ±5° and that thickness can be measured with an accuracy of about ±0.3 μm.

By measuring spectra of gem quality spessartine-almandine garnets using the microscope-spectrometric methods described above, as well as conventional macro-methods, showed the spectra obtained by the former to correspond to those of the later in all details (Langer – Abu-Eid 1977). In fact, the spectra obtained by microscope-spectrometry are in many cases, of better quality than those measured by conventional macro-methods, because optically clear parts in natural minerals may be smaller than beam dimensions in conventional spectrometers.

Recently, spectrometers based on interferometers and Fourier-transform evaluation of the interferograms without and with sample in the beam, first used in the infrared, were extended for measurements in the UV/VIS/NIR-ranges. Such instruments may be equipped with microscopes. To the author's knowledge, there are no spectra in the literature scanned with FT-interferometric spectrometers, which were obtained with the low effective beam diameters accessible in the equipment de-

scribed here. On the other hand, the advantage of interferometric instruments is that they need no wavenumber calibration and that measuring times may be very short, such that time resolved spectra can be obtained in favourable cases. One problem of the use of the interferometer principle at the relatively high energies, *i. e.* short wavelength of the spectral range mentioned above, is the constancy of the mirror drive. We used FT-microspectrometric methods in the VIS/NIR, because in this range the MCT-detectors used in such instruments are by far superior over the PbS-cells of our instrument, and found polarized spectra of olivines not always being reliable.

3. Results

Several of the topics compiled in Table 1, have been worked on by the author's group using microscope-spectrometry. Some examples of the results of such work will be given in the sections to follow. Other examples may be found elswhere (Langer 1984, 1988).

The first field mentioned in Table 1, the colour of minerals involves a complex interplay between the physics of the interaction of electromagnetic radiation the energies of which contain the range 25000–12500 cm^{-1}, *i. e.* the "visible", with mineral crystals in the transmitted or reflected mode – not treated here – on the one hand, and the physiological and psychological response of the observer on the other. Clearly, the first aspect is dominated by the absorption spectra – or reflection spectra, not treated here – of minerals as the minima and maxima of absorbance occurring in the spectra modulate the amplitudes $a(\bar{\nu})$ of the incoming radiation such that is reduced in certain ranges of $\bar{\nu}$. Sir William Henry Bragg (1862–1942) said once "Colour is produced by detroying colour".

This is clearly seen in the examples of garnet spectra displayed in Fig. 2. It is obvious from the absorption spectrum of pyrope in the VIS range that the low energy or red part of incident white light is allowed to pass through the crystal. Further, a minimum of absorbance though at a higher level of absorbance compared to the low one in the red, occurs slightly above 20000 cm^{-1}, *i. e.* in the blue. The result is a deep red colour with a slight blue hue, typical of the colour of pyrope perceived by our eye and mind. The intensity of the blue hue depends on the absorbance in the minimum ocurring slightly above 20000 cm^{-1}. Clearly, this height will depend on the absorbancies contributed by the contributions of the low-energy wing of the absorption edge along the slope of the spectrum of the pyrope crystal studied (*cf.* Fig. 2). The spectrum of uvarovite, on the other hand, shows that – as Bragg would eventually say – the red is "destroyed" by the low-energy wing of the band with a maximum near 16500 cm^{-1}, while the blue is "destroyed" by the band with a maximum near 23000 cm^{-1}. As a result, the colour of the transmitted light is dominated by the absorbance minimum near 19000 cm^{-1}: the mineral is green. Note that, in both minerals, the colours of which look so different, the origin of the two bands governing the transmittance in the visible, is the same dd-sa transitions of octahedral Cr^{3+}; the only difference is that the energies of the two bands are higher in pyrope than in uvarovite (Fig. 2).

The properties of absorption spectra and their relations to colour type and intensity may be quantized to obtain the CIE (x, y) chromaticity diagrams of the Internationale d'Eclairage (see introductory chapters of Peckett 1992). A large number of extended studies, most of which were done using conventional macro-scale spectrometry, was so far devoted to the colour of minerals (*e. g.* Platonov 1976, Nassau 1983). It is not the aim of this paper to discuss the related phenomena more lengthly.

3.1 Band assignment

Using the approach (B), introduced above, namely the study of synthetically grown mineral crystals containing only one type of centres that can be excited in the UV/VIS/NIR ranges, the dd-transitions of nearly all the $3d^N$-ions in many structural matrices could be identified with certainty. Table 2 gives an overview of systems studied by this approach by the author's group. For the details which concern low-symmetry band splittings, band polarizations and crystal field parameters, the reader is referred to the original literature cited in the Table. Only two examples will be discussed:

Fig. 8 reproduces single-crystal spectra of synthetically grown end-member garnet crystals, almandine, spessartine and andradite (Frentrup – Langer 1982) which contain $Fe^{2+[8]}$, $Mn^{2+[8]}$ or $Fe^{3+[6]}$, respectively, as the only transition-metal ion. Moore – White (1972) attempted to solve the assignment problem of dd-sf transitions caused by such ions in garnets using the above approach (C), tracing the concentration dependencies of band intensities. Our results prove that several bands, marked by arrows in Fig. 8, are to be reassinged as originating from dd-sf in $Fe^{2+[8]}$ in almandine, $Mn^{2+[8]}$ in spessartine or $Fe^{3+[6]}$ in andradite. In the case of end-member almandine and spessartine, this was also confirmed by the high-pressure behaviour of the marked bands that was in accordance with the energy shifts of the respective excited terms in the applying Tanabe-Sugano diagrams (Smith – Langer 1983).

The first attempt to experimentally model $Fe^{2+}Fe^{3+}$ charge-transfer in orthopyroxen was made by Steffen *et al.* (1988) who synthesized single crystals of a $Fe^{3+[6]}Al^{3+[4]}$-substituted ferrosilite with 10 mole % of the $Fe^{3+[6]}Al^{3+[4]}$ end-member at 1000 °C and 20 kbar. Such crystals were used to obtain polarized single-crystal spectra which showed (aside dd-sa of Fe^{2+}) a band typical of MM-CT, polarised along [001] and centered at 12500 cm^{-1}. From distance-band-energy relations, the band was assigned to charge-transfer between Fe^{2+} in M(2) and Fe^{3+} in M(1).

Another attempt to confirm by approach (B) the assignment of MM-CT excitation was made by Khomenko *et al.* (1994): Yellow to orange pyrope-almandine-grossular garnets typically occurring in diamondiferous

Table 2. Assignements of spin-allowed and spin-forbidden dd-ransitions of $3d^N$-ions in oxygen-based phases based on synthethic crystals with one type of $3d^N$-ion.

N	Ion	[CN]	Transition	Structural Matrix	Literature
1	Ti^{3+}	6	sa	rutile	Khomenko *et al.* (1996, 1998)
	V^{4+}	6		zircone	Langer and Jansen (unpubl.)
3	Cr^{3+}	6	sa, sf	kyanite	Langer (1984)
				clinopyroxene	Abs-Wurmbach *et al.* (1985)
	Mn^{4+}	6	sa, sf	in isolated octahedra of $Mn(SeO_3)_2$	Wildner – Langer (1994)
4	Cr^{2+}	4+2	sa, sf	Cr_2SiO_4	Furche – Langer (1998)
	Mn^{3+}	6	sa, sf	andalusite	
				(viridine)	Abs-Wurmbach *et al.* (1981)
				garnet	Frentrup – Langer (1981)
					Langer – Lattard (1984)
				clinozoisite	Langer *et al.* (1976)
				(piemontite)	Kersten et al. (1988)
				clinopyroxene	Weyer – Langer (unpubl.)
				kyanite	Langer (unpubl.)
5	Mn^{2+}	8	sf	spessartine	Frentrup – Langer (1982)
	Fe^{3+}	6	sf	andradite	Frentrup – Langer (1982)
				acmite	Langer – Abu-Eid (1977)
6	Fe^{2+}	6	sa, sf	orthopyroxene	Steffen *et al.*(1988)
		8	sa, sf	almandine	Frentrup – Langer (1982)
7	Co^{2+}	6	sa, sf	buetschliite and zemannite-type selenites	Wildner – Langer (1994)
8	Ni^{2+}	6	sa, sf	Ni, Mg-olivines	Hu *et al.* (1990)
9	Cu^{2+}	6	sa	chalcocyanite	Wildner, Langer, Giester (unpubl.)

kyanite-eclogite xenoliths from Yakutian kimberlites show in their spectra a strong and broad absorption band centered at 23500 cm^{-1} which is attached to the absorption edge (Matsyuk *et al.* 1985). Spectra measured on a series of such garnets which differed in the first instance in their Fe^{2+}- and Ti^{4+}- contents, are displayed in the upper left part of Fig. 9 (Platonov *et al.* 1991). The upper right part of Fig. 9 proves the intensity of the band at 23500 cm^{-1} to linearly increase with increasing concentration product $x_{Fe} \cdot x_{Ti}$, where x is the number of atoms per formula unit. This relation and the large half width of about 7000 cm^{-1} has led to the assignment of the band to $Fe^{2+[8]}$-$Ti^{4+[6]}$ charge transfer (Platonov *et al.* 1991). This assignement was confirmed (Khomenko *et al.* 1994) using approach (B), with the help of pure Ti, Fe-substitued pyropes, grown synthetically under controlled oxygen fugacities at 1000 °C and total pressures between 20 and 30 kbar. Spectra of such garnets, having an orange-brownish colour, exhibit the same band centered at 23000 cm^{-1} as the natural garnets (lower left part of Fig. 9). Also, the intensity is linearly correlated with the concentration product $x_{Fe} \cdot x_{Ti}$.

3.2 Spectroscopic determination of $3d^N$-concentrations in minerals

It is obvious from the foregoing discussions that each $3d^N$-ion in a specific structural matrix gives rise to a specific band or set of bands. It is also obvious that the intensities of bands characteristic of a specific ion, are related to the number of these ions per unit volume of the matrix, *i. e.* the ion's concentration

$$\alpha_{\bar{\nu}\,max} = f(c) \qquad (15)$$

with c = concentration of the ion in [g-atom · l^{-1}]. The function f in eqn. (15) is often of first order, especially in case of low concentrations, such that

$$\alpha_{\bar{\nu}\,max} = \varepsilon_{\bar{\nu}\,max} \cdot c \qquad (16)$$

with e a constant, the decadic molar absorptivity in [$l \cdot$ g-atom$^{-1} \cdot$ cm^{-1}]. Eqn. (16) is known as Beer's law. Provided, spectra of proper calibrational crystals with known concentration of the respective $3d^N$-ion have been measured, $e_{\bar{\nu}\,max}$ can be obtained from

$$\varepsilon_{\bar{\nu}\,max} = (\alpha_{\bar{\nu}\,max} \cdot V_{el} \cdot N_L) / (1000 \cdot X_{ion} \cdot Z) \qquad (17)$$

with V_{el} = the unit cell volume of the mineral structure in [cm^3], N_L = Avohadro's number in [$mole^{-1}$], X_{ion} = number of absorbing species per formula unit, and Z = number of formula units per unit cell. Eqns. (15) to (17), or the corresponding formalism using the integral instead of the linear absorption coefficient in [cm^{-2}]

$$\alpha_{int} = \int_{\bar{\nu}_1}^{\bar{\nu}_2} \alpha \, d\nu = t^{-1} \cdot \int_{\bar{\nu}_1}^{\bar{\nu}_2} (\log(I_o/I)\, d\bar{\nu} \qquad (18)$$

form the basis for spectroscopic concentration determinations, provided correct band assignments are known. These determinations can be performed on areas of the crystal down to diameters of about 5 mm and have the great advantage that they are valence-specific. If the band or bands used for the determination do not occur too far towards the UV where emdedding materials start to absorb, then determinations can be done on mineral grains in thin section.

Examples for the calibration of eqn. (16) for divalent manganese and ferrous iron in garnets on the basis of single-crystal spectra of synthetic garnet endmembers and binary solid solutions (Frentrup 1980) are presented in Fig. 10. In both cases, the spectral properties, which are evaluated to obtain the $\alpha_{\bar{\nu}\,max} = f(c)$ relation, are defined on the left side of the Figure. The crystals of garnet endmembers and binary solid-solutions, on which the spectra were measured, have been grown up to sizes of 500 µm diameter, mostly at 25 kbar and 900 °C, and their composition was checked by electron microprobe analyses (Frentrup 1980). When we consider that the zero-point of the linear calibrations of Fig. 10 corresponds to $Mn^{2+[8]} = 0.00$ or $Fe^{2+[8]} = 0.00$ per formula unit and the uppermost points to 3.00 pfu in both cases, then we realize from the errors given in the Figure, that microscope-spectrometric determinations of Mn^{2+} and Fe^{2+} in garnets are possible with an accuracy of about ±0.20 cations per

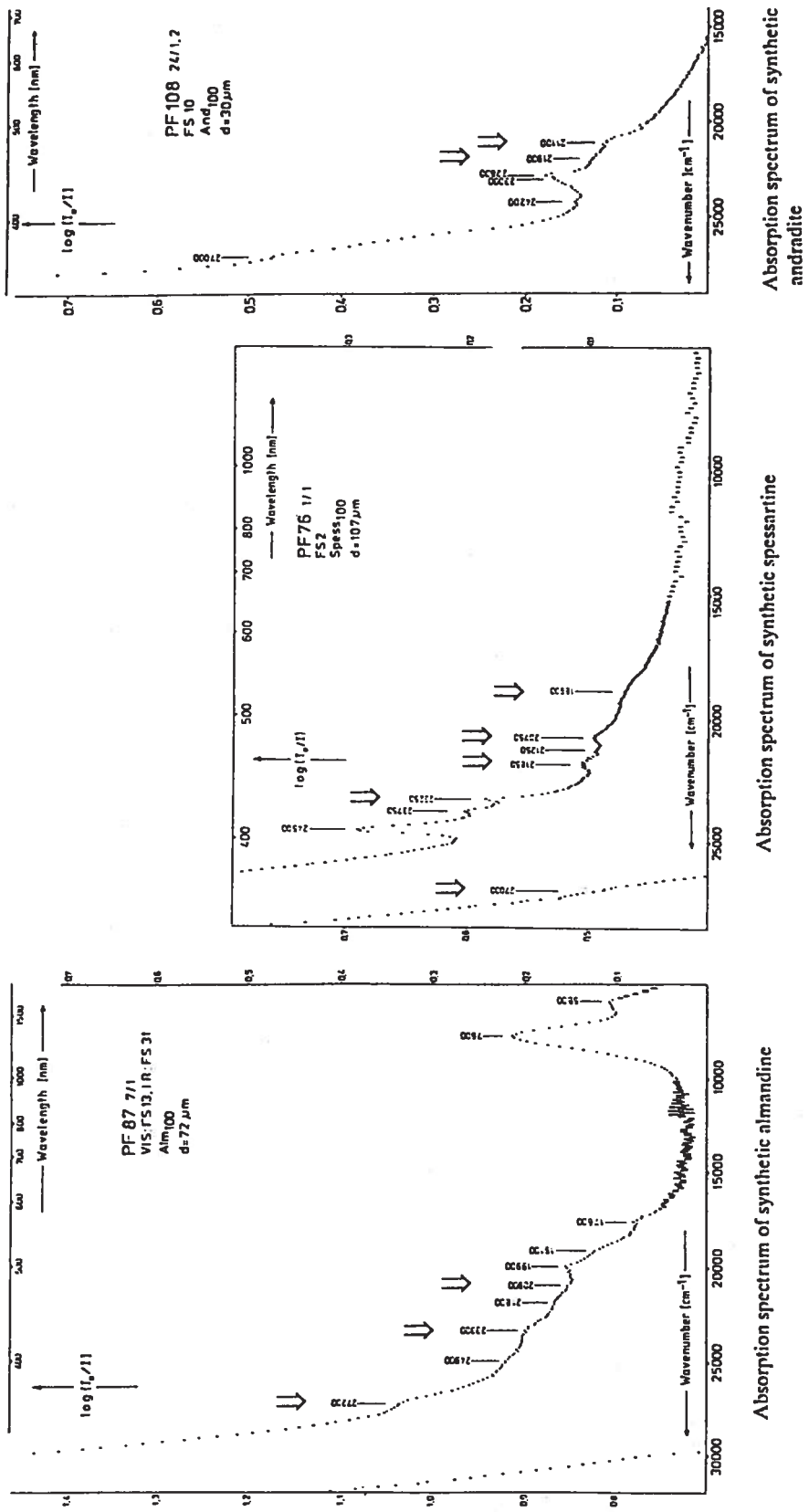

Fig. 8. Single crystal spectra of the synthetic garnet end members almandine, spessartine and andradite. The arrows mark those bands that are newly identified as spin-forbidden bands of Fe^{2+}, Mn^{2+} or Fe^{3+} in garnet.

– allocation of small amounts of Fe^{3+} in synthetic orthoferrosilite in M(1) octahedra (Steffen *et al.* 1988)

– allocation of small amounts of Ti^{4+} in ellenbergerite (Chopin – Langer 1988) and in dumortierite (Platonov *et al.* 2000) in face connected octahedra forming chains parallel to [0001]of the structures.

Bands caused by dd-sa transitions of $3d^N$-ions can be used to solve the problem of intersite fractionation of the respective $3d^N$-ion and the one for which it subsitutes in multisite structures of solid solutions. The presupposition is that the sites involved in the intracrystalline fractionation process

$$M_{3d^N}{}^{n+}(M1) + M^{n+}(M2) \leftrightarrow M^{n+}(M1) + M_{3d^N}{}^{2+}(M2) \quad (19)$$

are sufficiently different in their geometry, point symmetry, distortion and mean ligand-metal distances R_{M-O}. In this case, two sets of bands to be expected from the are $3d^N$-ion in either M1 or M2 can be identified and separated in the spectrum of the mineral. This is the case for M1 and M2 in orthopyroxenes. Thus, Goldman – Rossman (1977) were successful in determining the site fractions $x_{Fe\ M1}$ and $x_{Fe\ M2}$ in osthopyroxenes from the intensities of the respective sets of dd-bands which could be identified because 10Dq and the low-symmetry splitting

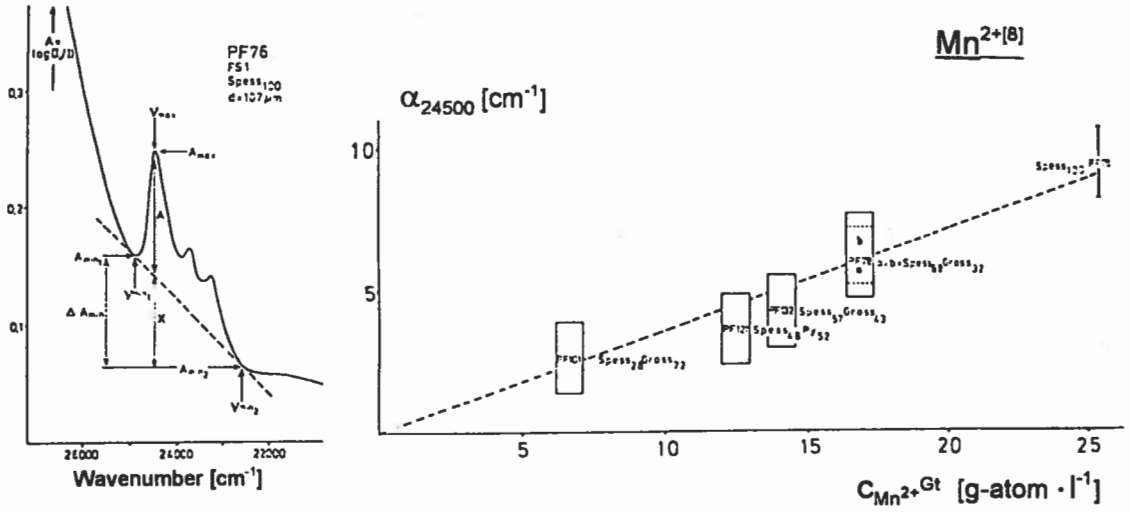

$$\alpha_{24500} = A/t = (A_{max} - A_{min2} - x)/t$$

$$x = (A_{min1} - A_{min2})(\bar{\nu}_{max} - \bar{\nu}_{min2})/(\bar{\nu}_{min1} - \bar{\nu}_{min2})$$

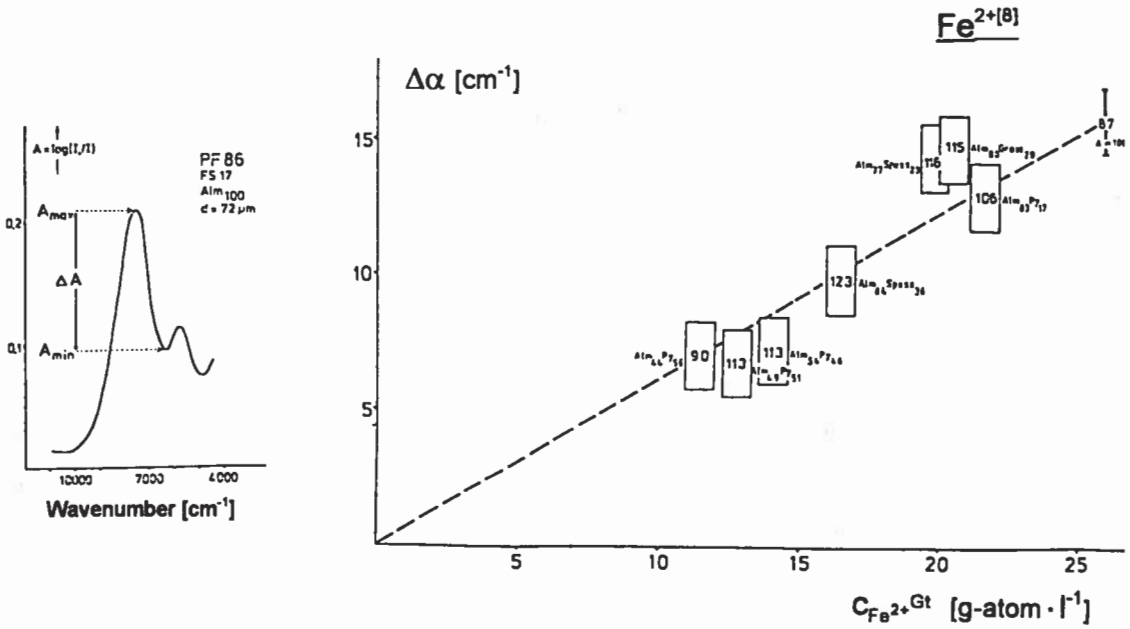

$$\Delta\alpha = [A_{max,\ 7600} - A_{min,\ 6500}]$$

Fig. 10. Calibrations of spectroscopic properties for microscope-spectrometric Mn^{2+}- or Fe^{2+}-determination in garnets.

greatly differs in the two sites in the orthopyroxene structure.

We measured the polarized single crystal spectra of flux grown Ni, Mg-olivines, $(Mg_{1-X}Ni_X)_2SiO_4$, with different X. Two sets of bands originating from Ni^{2+} in the centrosymmetric M1-sites with their small R_{M1-O} or in the non-centrosymmetric M2-sites with larger R_{M2-O} could be identitfied (Hu *et al.* 1990). Fig. 11 displays polarized spectra with E||X(||b), E||Y(||c) and E||Z(||a) on crystals with X_{Ni} = 0.02, 0.30, 0.75 and 1.00. Orientations are given adopting the Pbnm space group of the olivine structure (Bragg – Brown 1926). Hu *et al.* (1990) showed that there are two sets of Ni^{2+} dd-sa bands, bands a, e, h originating from Ni in M1 and bands b, g plus a band in the range i, j, originating from Ni in M2. The other, weak and partly sharp bands showing up in the spectra of Fig. 11, could be assigned to dd-sf bands of Ni in M1 or M2 on the basis of the Tanabe-Sugano diagram of this $3d^8$-configurated ion. Further, it was shown that the linear absorption coefficient of the strong band b of Ni in M2, together with the bulk Ni-content X_{Ni} are sufficient to determine the site fractions of Ni in the two M-sites, $x_{Ni\,M1} = [n_{Ni}/(n_{Ni}+n_{Mg}]_{(M1)}$ and $x_{Ni\,M2} = [n_{Ni}/(n_{Ni}+n_{Mg})]_{(M2)}$, for any composition,with the presupposition that Beer's law is valid, *i. e.* that the function $\alpha_b = f(x_{NiM2})$ has the form $\alpha_b = \varepsilon_b \cdot x_{Ni\,M2}$. Then

$$x_{Ni\,M2} = \alpha_{b\,x}/\alpha_{b\,(x=1)} \qquad (20)$$

and

$$x_{Ni\,M1} = 2X_{Ni} - x_{Ni\,M1} \qquad (21)$$

The site fractions obtained by evaluating the polarized spectra in such a way, are plotted in the partitioning diagram of Fig. 12 along with data obtained by structure refinements of (Ni, Mg)-olivines (Boström 1987). The plot shows that the two methods yield data sets that agree quite well. At the temperature of about 900 °C, at which the flux-growth experiments of the crystals are very likely to be frozen in during quenching (Boström 1987), Ni^{2+} fractionates predominantely into the centrosymmetric, smaller M1-sites, a result to be expected from size and non-degenerate crystal field ground state of Ni^{2+} (*cf.* middle part of Fig. 4). The obvious power of the spectroscopic method encouraged to use it as a tool in a kinetic study of the intracrystalline cation-exchange reaction, eqn. (19), after the validity of Beer's law in the whole compositional range 0<X<1 was confirmed by a series of new structure refinements and polarized spectra on a set of newly grown Ni,Mg-olivine crystals (Garsche 1994, Garsche – Langer 1994). Results of this work will be published elsewhere (Garsche – Langer, in prep.).

3.4 Intercrystalline partitioning and crystal- field stabilization energy of $3d^N$-ions

If the crystal-field stabilization energy of a $3d^N$-ion (*cf.* section 1.2, part 3) in the respective polyhedra of the structures of different paragenetic, coexisting oxygen-based minerals has different values, then it might be expected that in the equilibrium state of intercrystalline exchange processes, the $3d^N$-ion will fractionate predominantely into that mineral phase where $CFSE_{3d}N$ is highest. This concept (Burns *et al.* 1964, Merlino 1965), the crystal-field-concept CFC (Langer and Andrut 1996), found much qualitative evidence (Burns 1970, 1993). Only recently, it was attempted to check for the validity of CFC by search for quantitative relations of the type

$$c_{3d^N} = f\,(CFSE_{3d^N}) \qquad (22)$$

or

$$K_{D,\,3d^N,\,T}^{(Ph1/Ph2)} = f(\Delta CFSE^{(Ph1-Ph2)}) \qquad (23)$$

Clearly, a presupposition to find such relations is that minerals are studied which are in equilibrium with respect to intercrystalline $3d^N$-partitioning, such that T in eqn. (23) is fixed. This is the case in paragenetic minerals which should then be the objects of study to find quantitative relations of the type of eqns. (22) and (23) as a proof of the validity of CFC.

The intercrystalline partitioning of two geoscientifically important $3d^N$-ions which can be regarded as extreme cases are studied with the approach of paragenetic minerals, the $3d^3$-ion Cr^{3+} (Langer – Andrut 1996) and the $3d^6$-ion Fe^{2+} (Langer – Khomenko 1999).

The distribution of Cr^{3+} between pairs of minerals of six parageneses, *gt/cpx/ky, gt/cpx/amph, cor/parag/phlog, cor/ky/ms* and a *cpx/opx*-exsolution, has been studied by electron microprobe analysis and polarized single crystal spectroscopy. In all cases except for the exsolution, quantitative relations of the types of eqns. (22) and (23) were found. This led to the conclusion that in the case of Cr^{3+} CFC is valid, as the intercrystalline partitioning behaviour is ruled by the ion's crystal field stabilization.

The distribution of Fe^{2+} was studied in a similar way using ten parageneses extracted from precambrian rocks of the Unkrainian shield, three different parageneses *gt/opx/cpx*, and one paragenesis of each, *Ca-amph/bio, gt/opx/bio, gt/bio, gt/cord, gt/cord/bio, gt/opx/cpx/Ca-amph, gt/cpx*. Other than in the case of Cr^{3+}, clear relations of the type of eqns. (22) and (23) were only observed when geometrical factors, mainly polyhedral volumes in the respective mineral structures and radii of the ions competing in the partioning process, are similar in the respective two paragenetic mineral phases to within 15–20 %. In such cases, the $\Delta CFSE_{Fe}2+$ contribution to $K_D^{(Ph1/Ph2)}$ amounts to about 0.1–0.2 log K_D per 100 cm^{-1} ΔCFSE. The conclusion is that in the case of Fe^{2+}, crystal field stabilization plays only a secondary role after geometrical factors.

The reason for the great difference in the influence of $CFSE_{3d^N}$ on the $3d^N$-ion partitioning is seen in three factors (Langer – Khomenko 1999): (i) $Dq_{Cr^{3+}} = 3 \cdot Dq_{Fe^{2+}}$ (*cf.* middle part of Fig. 4), (ii) the values of 10Dq differ greatly (*cf.* eqn. (12)), $10Dq_{Cr^{3+}} \cong 1.85 \cdot 10Dq_{Fe^{2+}}$ and (iii) Cr^{3+} enters exclusively octahedral sites with similar geometrical properties in the paragenetic mineral phases.

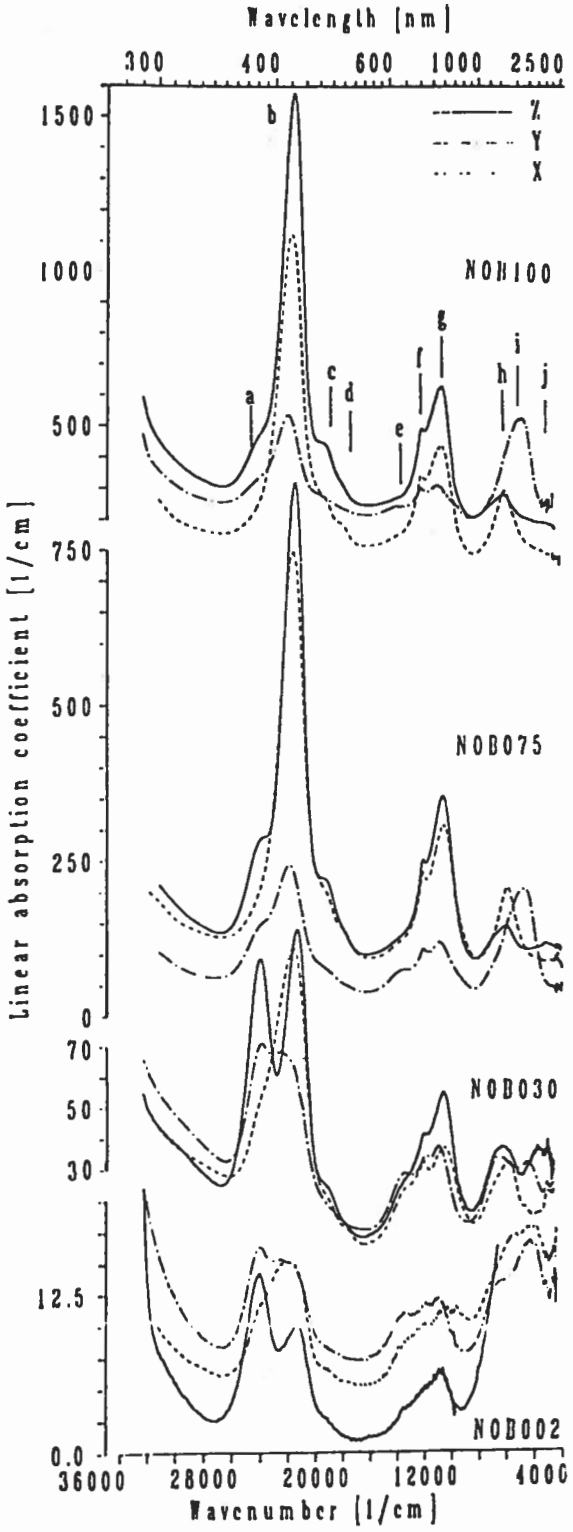

Fig. 11. Polarized single crystal spectra of flux grown (Mg,Ni)-olivine single crystals, $(Mg_{1-X}Ni_X^{2+})_2[SiO_4]$, with different X_{Ni} showing spin-allowed and spin-forbidden dd-transitions of Ni^{2+} in olivine M1 and M2 sites.

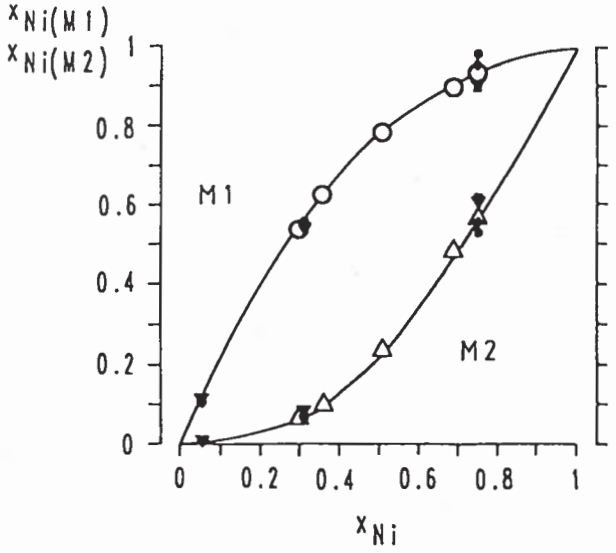

Fig. 12. Variation of site fractions of nickel, x_{Ni}, in octahedral M1 and M2 sites in olivine-type $(Mg_{1-X}Ni_X^{2+})_2[SiO_4]$ at 1173K as a function of bulk nickel contents, X_{Ni}. Open symbols and solid curves: data from structure refinenments (Boström 1987), closed symbols: data from polarized sinngle crystal spectra (Hu *et al.* 1987). or nickel site fractions from α_{lin} in spectra with E||X or E||Z, respectively, or nickel site fractions from α_{int} in pectra with E||X or E||Z, respectively.

3.5 Local structal properties - crystal defects: UV-spectra and fO_2–T-dependent Fe^{3+}-bearing point defects in olivines

Inside the fO_2–T-stability field of fayalite and Mg, Fe-olivine solid solutions (Nitsan 1974), increasing fO_2 – at constant temperature T – will produce an inceasing concentration of Fe^{3+}-bearing point defects in the structure, which are introduced as majority defects by the reactions

$$6Fe_{M(1,2)}^{x} + SiO_2 + O_2 = 4Fe_{M(1,2)}^{\bullet} + 2V_{(M1,2)}'' \quad (24)$$

$$Fe_{M(1,2)}^{x} + Si_{Si}^{x} + (1/2)Fe_2SiO_4 + (1/2)O_2 = Fe_{M(1,2)}^{\bullet} + Fe_{Si}' + (3/2)SiO_2 \quad (25)$$

(Nakamura – Schmalzried 1983). These eqns. use the point defect notation proposed by Sockel *et al.* (1974): $Fe_{M(1,2)}^{\bullet}$ = Fe^{3+} in octahedral sites ("defect electrons"), $V_{M(1,2)}''$ = vacancies on octahedral sites (two non-compensated negative charges), Fe_{Si}' = Fe^{3+} on tetrahedral Si-sites (one non-compensated negative charge), ^{x} designates normal occupation of the respective sites (no extra positive or negative charge). By means of an ultrasensitive gravimetric method, Nakamura – Schmalzried (1983) determined weight changes $\pm\delta$ of a fayalite crystal, connected with eqns. (24) and (25), as a function of temperure and oxygen fugacity. From these, they evaluated the equilibrium constants of the defect reactions, and their tem-

perature dependencies. Using such data, it is possible to calculate for various temperatures, the site fractions of Fe^{3+}

$$x_{Fe}\cdot = [Fe_{M(1,2)}\cdot] + [Fe_{M(1,2)}\cdot\ Fe_{Si}{}'] \qquad (26)$$

at any fO_2 inside the fO_2–T-stability field for fayalite and olivines or, vice versa, to calculate fO_2 of olivine formation from $x_{Fe}\cdot$. Clearly, this latter possiblity is of high impertance in mantle geochemistry and, hence, availability of a simple method for determining $x_{Fe}\cdot$ was desirable.

In search of a microscope-spectrometric method suitable for this purpose (Čemić *et al.* 1986), we estimated the effect of O^{2-}-Fe^{3+} LM-CT bands (Tossell *et al.* 1974, *cf.* eqn. (7)) originating from Fe^{3+}- bearing point defects for site fraction in fayalite $x_{Fe}\cdot = 1.7 \cdot 10^{-4}$ (800 °C / fO_2=1.86 · 10^{-17}atm), adopting molar absorptivities of LM-CT bands of Fe^{3+}- or Fe^{2+}-oxygen-based complexes as found by Lehmann (1970). The results are shown in the left part of Fig. 13. The very small fraction of Fe^{3+} will cause the UV-edge, otherwise dominated by O^{2-}-Fe^{2+} LM-CT, to shift slightly to lower energy. In order to prove such an effect and, if this would be successful, to calibrate $\alpha_{X,Y,Z(\bar{\nu})}$ against $x_{Fe}\cdot$, a set of fayalite single crystal was needed with the following properties: (i) defined $x_{Fe}\cdot$, homogeneous distribution of Fe^{3+} in the crystals, (ii) longest dimension not smaller than about 100 μm, such that individual crystals could be manipulated in the preparation of crystallographically oriented platelets, (iii) known $x_{Fe}\cdot$. Fayalite single-crystals fulfilling points (i) and (ii) were grown at 800 °C/ 10kbar in the presence of water under the defined oxygen fugacities of the oxygen buffers (in parentheses: fO_2 at 800 °C in atm) FeQu/Fa (4.68 · 10^{-20}), Fe/Wu (4.90 · 10^{-19}), Wu/Mt (1.86 · 10^{-17}) and Fa/MtQu (1.86 · 10^{-14}). Point (iii) was achieved by calculating the $x_{Fe}\cdot$ -values for the different fO_2 using the Nakamura – Schmalzried (1983) data (for the formalism *cf.* Čemić *et al.* 1986). From the E||Z spectra shown in the right part of Fig. 13, it is obvious that the theoretically deduced effect does really occur though it is only small, due to the very low Fe^{3+}-concentrations which are calculated to be in the range $0.62 \cdot 10^{-4}$ (FeQu/Fa) < $x_{Fe}\cdot$ < $5.27 \cdot 10^{-4}$(Fa/MtQu). The effect was also observed in the E||X and E||Y spectra and has been calibrated for all three polarizations using up to six different crystals grown under same conditions. This resulted in the linear calibrational relations

$$\alpha_{X\ 26500} = 107191 \cdot x_{Fe}\cdot + 647.0 \text{ (with r = 0.999)} \quad (27)$$
$$\alpha_{Y\ 26500} = 69468 \cdot x_{Fe}\cdot + 505.5 \text{ (with r = 0.93)} \quad (28)$$
$$\alpha_{Z\ 28000} = 165804 \cdot x_{Fe}\cdot + 640.6 \text{ (with r = 0.993)} \quad (29)$$

These calibrations, together with the calculational procedure to obtain fO_2 from $x_{Fe}\cdot$, allow the determination from single-crystal spectra in the UV, of the oxygen fugacity of olivine formation in nature. The problem in transferring eqns. (27) to (29) from faylite to olivines $(Mg_{1-X}Fe_X)_2SiO_4$ with X < 1.00 is that the UV edge is not only influenced by $x_{Fe}\cdot$ but also by the bulk X_{Fe}. As long as X_{Fe} is the same in olivines of different origin, relative fO_2-values for the different olivines can be estimated

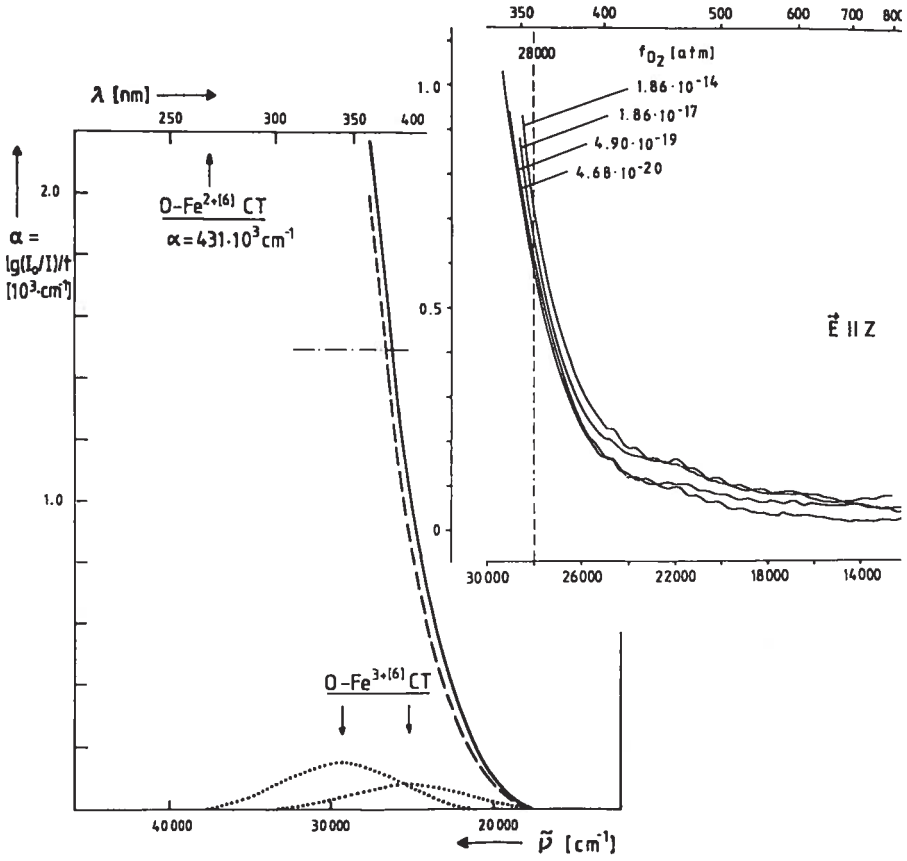

Fig. 13. UV absorption edge of faylite containing Fe^{3+}-bearing point defects: left part, calculated edge for an iron(III) site fraction of $x_{Fe}\cdot = 1.7 \cdot 10^{-4}$ (full line), right part: the edge in measured spectra of fayalites grown under the oxygen fugacities indicated. Note that the slope of the edge, calculated as the sum of that in pure Fe^{3+}-free fayalite (dashed line) and the contribution from O-Fe^{3+} CT to this (dotted lines), shows a red shift compare with that of defect-free fayalite and note that a red shift is also obvious on increasing oxygen fugacity in the experimental spectra (*cf.* text).

from their UV-spectra (Khisina *et al.* 1992). In case of olivines with different X_{Fe}, the influence of such differences can be overcome (Dyar *et al.* 1996) by correcting the $\alpha_{X,Y,Z\,(\bar{\nu})}$-values obtained from the respective spectra, for the contribution of X_{Fe} using data from UV spectra of a series of synthetically grown olivine crystals with different X_{Fe} (Smith – Langer 1981).

3.6 Local structural properties: local mean distances

When in an oxygen-based crystalline solid solution, a small metal ion M_A in a coordination polyhedron i with coordination number n is substituted by a larger metal ion M_B, then the crystal- averaging diffraction methods of structural research will yield mean $\bar{R}_{(M\text{-}O)\,i}$-distances equal or close to the function interpolating the repective end member values, $\bar{R}_{(MA\text{–}O)\,i}^{\circ}$ and $\bar{R}_{(MB\text{–}O)\,i}^{\circ}$, as shown by the dashed line in Fig. 14 (Vegard's rule). However, such experimental results cannot be the truth as far as the local mean $\bar{R}_{(M\text{–}O)\,i}$-distances, *i. e.* the distances in the individual M_A- or M_B-centered polyhedra of type i are concerned. Such statement seems trivial, as the validity of Vegard's rule on a local polyhedral scale would imply that there is no relaxation of the structure near to substituted polyhedra and any strain connected with the substitution is taken up by the substituting M_B-ions by radius changes or by the smaller M_A by "rattling" in the polyhedra i. The opposite possibility is that any strain involved in the substitution is fully relaxed in the structure such that the two ions M_A and M_B behave as completely hard spheres. In this case, the mean distances $\bar{R}_{(MA\text{–}O)\,i}$ and $\bar{R}_{(MB\text{–}O)\,i}$ are represented by the dotted lines in Fig. 14. The averaged values, obtained by structure refinement using diffraction methods, will then be fractional sums of such hard-sphere distances. This is unlikely for energetic reasons (Urusov 1992). An intermediate model involving partial lattice relaxation, as shown by the solid lines in Fig. 14, seems to be the adequate one. Urusov (1992) proposed to characterize the degree of lattice relaxation on a geometrical basis by the quantity ε which is with the notation of Fig. 14, given by

$$\varepsilon = (\bar{R}_{(MB\text{–}O)\,i}^{\,local} - \bar{R}_{(MA\text{–}O)\,i}^{\circ}) \,/\, (\bar{R}_{(MB\text{–}O)\,i}^{\circ} - \bar{R}_{(MA\text{–}O)\,i}^{\circ}) \quad (30)$$

such that for full relaxation ε = 1.00 and for absent relaxation ε = 0.00.

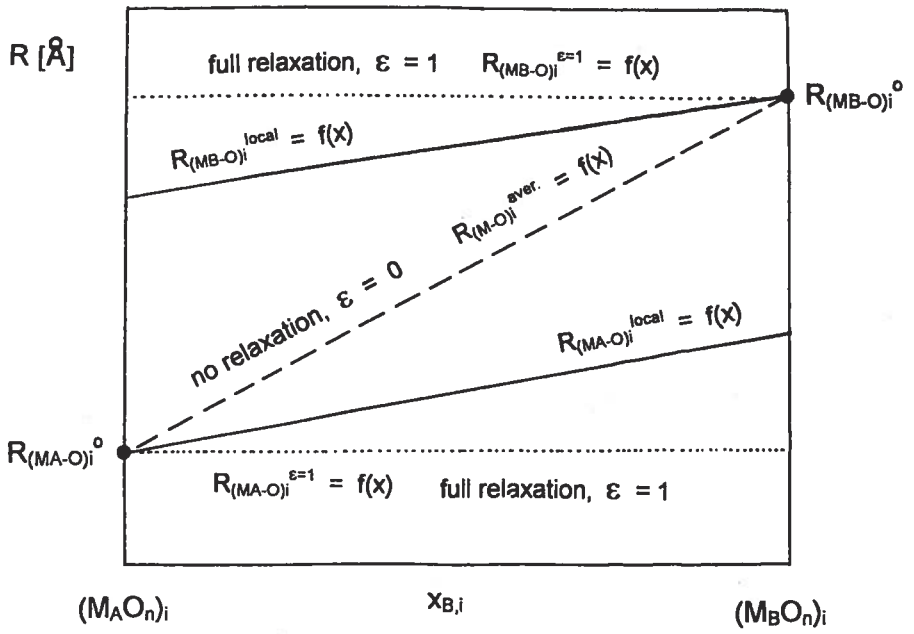

Fig. 14. Mean metal-oxygen bond lengths in $(M_{A\,(1-x)}\,M_{B\,x})$ – substituted polyhedra i as a function of substittutional degree x_B (cf. text).

Evalution of the dependence of $10Dq_{3d^N}$ on mean M-O distances as given by eqn. (13) yields experimental local distances at $x_{B,i}$ (Fig. 14), provided values of 10Dq and $\bar{R}_{(M\text{–}O)\,i}^{\circ}$ for the $3d^N$-ion bearing end-member can be measured or are otherwise available. Then, we derive from eqn. (13)

$$\bar{R}_{(MB\text{–}O)\,i,x}^{\,local} = \bar{R}_{(MB\text{–}O)\,i}^{\circ} \cdot (10Dq_{MB}^{\circ}/10Dq_{MB,x})^{1/5} \quad (31).$$

M_B is the substituting $3d^N$-ion. The index ° or subscript $_x$ designate the M_B end-member values or those of the solid solutions with substitutional degree $x_{B,i}$ in the polyhedra of type i, respectively. Eqn. (31) holds for both cases, $\bar{R}_{(MB\text{–}O)i}^{\circ} > \bar{R}_{(MA\text{–}O)i}^{\circ}$ (Fig. 15) and $\bar{R}_{(MB\text{–}O)i}^{\circ} < \bar{R}_{(MA\text{–}O)i}^{\circ}$. In this way, octahedral local transition metal-ion - oxygen distances were calculated as a function of the substitutional degree x_{3d^N} (Langer 1988, 1999) from existing spectroscopic and structure refinement data for the substituted octahedra in the following solid solutions

Viridine, $(Al_{1-X}Mn_X^{3+})_2[O|SiO_3]$
M1-octahedra, $[(Al_{1-x}Mn_x^{3+})O_6]_{M1}$

Piedmontite, $(Al_{1-p}Mn_p^{3+})_3[OH|O|SiO_4|Si_2O_7]$
M3-octahedra, $[(Al_{1-x}Mn_x^{3+})O_6]_{M3}$

Corundum, $(Al_{1-X}Cr_X^{3+})_2O_3$
Al-octahedra, $[(Al_{1-x}Cr_x^{3+})O_6]_{Al}$

Chloritoid, $(Fe_{1-X}Mg_X)_2AlAl_3[O_2|(OH)_4|(SiO_4)_2]$
M1B-octahedra, $[(Mg_{1-x}Fe_x^{2+})O_4(OH)_2]_{M1B}$

Olivine, $(Mg_{1-X}Ni_X^{2+})_2[SiO_4]$
M1-octahedra, $(Mg_{1-x}Ni_x^{2+})O_6]_{M1}$

(data from: Abs-Wurmbach *et al.* 1981, Kersten *et al.* 1988, Khomenko – Langer unpubl., Koch-Müller *et al.* 2000, Garsche – Langer 1994). In all cases, structural relaxion around the local centers of substituted octehedra is obvious, *i. e.* $0 << e < 1$ is realized (Fig. 14). In case of $3d^N$-ions larger than the substituted spherical cation, as this is true for Mn^{3+}, Cr^{3+} and Fe^{2+} in the above solid solutions, then the $3d^N$-ion is cation B of Fig. 14 when it is smaller, then it is cation A of Fig. 14 as this is the case for Ni^{2+} in the above solid solutions. In the first case, a function f as shown for $\bar{R}_{(MB-O)i}^{local}$ in Fig. 14 is representative, in the second a function f as shown for $\bar{R}_{(MA-O)\,i}^{local}$. In any case, a Vegard-like function $\bar{R}_{(M-O)i}^{aver.} = f(x)$ as it is shown in Fig. 14 by the dashed line and as it is experimentally obtained by diffraction methods of structure research is realized only as a fractional sum of the two local distances.

3.7 Local structural properties: polyhedral compressibilities and polyhedral thermal expansion

In a way analog to the just described one for obtaining local mean M-O distances in $3d^N$-substituted polyhedra type i as a function of substitutional degree x_{3d^N}, local distances may be determined spectroscopically as functions of pressure p or temperature T while the substitutional degree x_{3d^N} is kept constant. This means, local polyhedral compressibilities and local polyhedral thermal expansions. These local properties may be obained from the respective pressure or temperature dependencies of $\bar{R}_{(M-O)i}$. Such changes may be calculated from changes in 10Dq on pressure or temperature, respectively, *i. e.* from an analysis of high-pressure or high-temperature spectra. This is obvious when the data characterised by index $^\circ$ in eqn. (31), are replaced by data characterised by ^{1atm} or ^{298K}, respectively, and those characterized by subscript $_x$ in eqn. (31) by such characterized by $_{p,kbar}$ or $_{T,K}$, respectively. The formalisms to obtain the polyhedral modulus, k_{poly}, or the polyhedral thermal expansion, α_{poly}, are given elswhere (Langer *et al.*1996, Taran *et al.* 1994, respectively).

Some typical examples of unpolarized spectra of Cr^{3+}-bearing minerals at random and at high pressure are displayed in Fig. 15. Polarized spectra of minerals of non-regular systems can be measured only up to some 20 kbar. Above this pressure, polarizations are mixed due to strain-induced birefringence of the diamond windows. Octahedral bulk moduli and polyhedral thermal expansions of some oxygen-based, Cr^{3+}-bearing minerals which we spectroscopically derived so far, are presented in Table 3. Such values agree within the limits of error with existing data from high-pressure X-ray structure refinement (column 5 of Table 3). Columns 6 and 7 of Table 3 compare the values of k_{poly} obtained from high-pressure spectra with the bulk moduli of the respective minerals. It is evident that in all cases k_{poly} is appreciably higher than k_{bulk} which indicates that other mechanisms than compression of octahedra are predominantely relaxing the stress from increas-

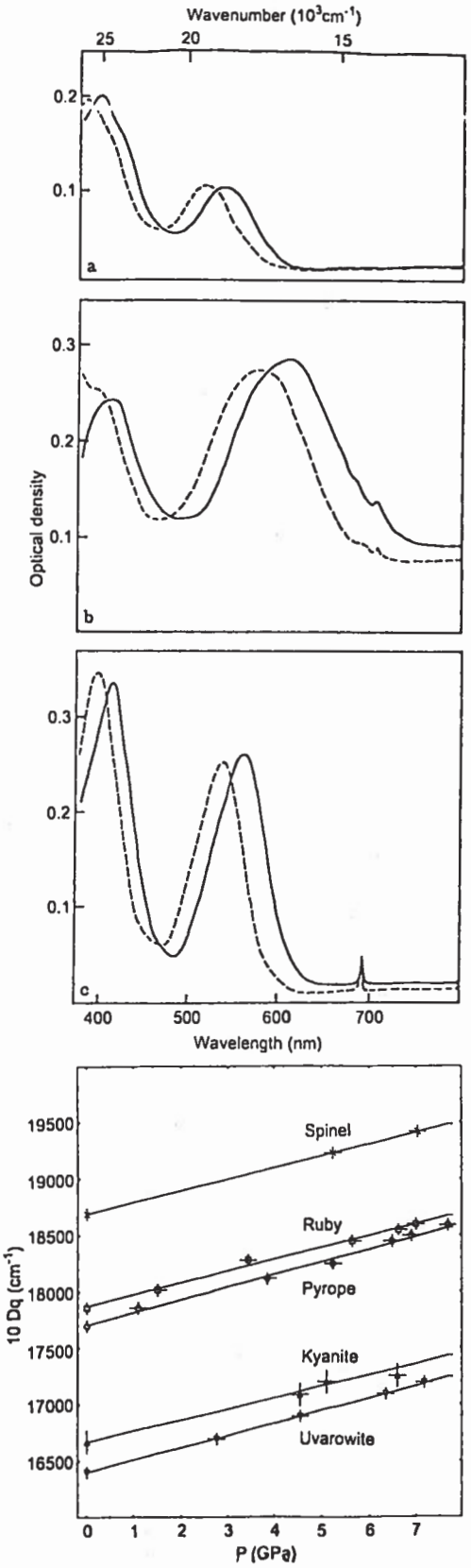

Fig. 15. Examples of single crystal spectra of Cr^{3+}– bearing mineral phases at ambient and high pressures (upper part) and pressure dependence of the crystal field parameter of Cr^{3+} in various mineral structures studied (lower part). The spectra from top to bottom are spinel up to 7.04 GPa, kyanite up to 6.60 GPa and ruby up to 7.01 GPa, dotted lines represent the high pressure spectra.

ing pressure, as compression of XO_8-triangular dodecahedra in garnet or polyhedral tilting in spinel. In case of ruby, the octahedral modulus, k_{poly}, obtained from high pressure spectra is close to the bulk modulus, which indicates that in this densely packed structure, octahedral compressibility is the most important mechanism of stress relaxation. The octahedral thermal expansion, derived from high-temperature spectra in pyrope and grossular, is higher the respective bulk property, while both α-values are the same within the limits of error in ruby and diopside.

4. Outlook

It is hoped that the foregoing demonstrates the power of electronic microscope-spectrometry to contribute to many fields of geosciences. For the microscopist, the possibility of determining the contents of transition metal ions (including their valencies, *e. g.* Fe^{2+} and Fe^{3+}) in minerals in thin section at an areal resolution similar to that of the electron-microprobe, will appeal. What is required is a monochromatizer in the entrance beam of a microscope and a photometric device (including the entrance and exit diagphragms) at the proper places in the beam path. The monochromator should be either a prism or a grating monochromator of sufficient spectral resolution; an interference filter is not suited in this respect. What else is required are proper calibrations. The problem is solved for Fe^{2+} and Mn^{2+} in garnets and for Fe^{2+} and Fe^{3+} in chloritoids, but other purposes need still calibrational work. It is hoped that this will be done as the possibility of determining transition metal-ion contents at N, *i. e.* their valencies at a high local resolution is most easily accessible by microscope-spectrometry.

The other applications discussed here, need special thinking and experimental set-up. In any case, further study by microscope-specrometry, of intracrystalline and intercrystalline $3d^N$-ion distribution as well as the elucidation of local polyhedral properties and of point defects in crystals may greatly contribute to our understanding of the crystal-chemistry and -physics of oxygen-based minerals.

Why do I all the time emphasize oxygen-based minerals, why not also sulfides, sulfosalts *etc.*? The reason is, that a theoretical approach is needed that allows us to extract data from the spectra, useful in our tasks. This is the case for the applicability of the crystal-field-/ ligand-field-theory to the interpretation of electronic spectra of oxygen-based minerals. There exists a saying of some, who are not so familiar with $3d^N$-ion spectroscopy and evaluation, that such theories are outdating now in view of the quantum mechanical ab-initio calculations accessible by now to the available big computers. However, this is nothing but prejudice as obvious from several facts: (a) Ligand-field theory is based on quantum mechanical calculations as well, (b) the quality of data derived by its semiempirical application is high as shown in the respective literature including this paper, (c) ab-initio calculations of spectra produce band energies and polarisations which are apart from observed values by 10 % or more (Krasovska *et al.*1997). This is fine when the difficulties of the calculations are considered, but it is bad when we think of the accuracy of data evaluated from spectra by the semiempirical use of the aforementioned theoretical approaches.

Aside of this, there are still some experimental problems in microscope-spectrometry to be solved or their existing solutions to be optimized: (i) meaurement of polarized spectra in the range of very high aborption, *e. g.* beyond 40000 cm^{-1}, (ii) measurement in the NIR, ca. 11000–4000 cm^{-1}, where low sensitivity of detectors cause often problems, (iii) measurements on small crystals with high refraction indices, causing problems by diffraction at the grain boundaries, esp. in the red and NIR, (iv) deconvolution of the spectra, asymmetry of "back-

Table 3. Local properties: Compression moduli and thermal expansion of $3d^N$-ion polyhedra from p- or T-dependent electronic spectra, respectively, of oxygen-based minerals. Spectroscopically derived data are compared with corresponding polyhedral data, where available, X-ray structure refinements at high p or T. Polyhedral compression moduli from spectra are also compared with bulk moduli.

Mineral	Ion	[CN]	Compression local $k_{poly,\ spectry}$ [GPa]	$k_{poly,\ XRD}$ [GPa]	bulk k_{bulk} [GPa]	$k_{poly,\ spectry}/k_{bulk}^{-1}$	Thermal Expamsion local $\alpha_{poly,\ spectry}$ [10^{-5} K^{-1}]	$\alpha_{poly,\ XRD}$ [10^{-5} K^{-1}]
Spinel	Cr^{3+}	6	312 ± 48 [1]		196.9 [2]	1.58	1.2 [3]	
Kyanite	Cr^{3+}	6	297 ± 70 [1]					
Ruby	Cr^{3+}	6	298 ± 44 [1]	250 ± 20 [4]	257 [5]	1.16	1.1 [3]	0.81–1.03 [6]
Pyrope	Cr^{3+}	6	275 ± 45 [1]	220 ± 50 [7]	175 [8]	1.57	1.5 [3]	0.79 [7]
Uvarovite	Cr^{3+}	6	257 ± 32 [1]		162 [8]	1.59	1.8 [3]	
Grossular	Cr^{3+}	6					2.0 [3]	1.3 [7]
Topaz	Cr^{3+}	6					0.6 [3]	
Diopside	Cr^{3+}	6					1.6 [3]	1.4 [6]
Almandine	Fe^{2+}	8	124 ± 25 [8]		178 [6]	0.70		
Pyrope	Fe^{2+}	8		130 ± 10 [9]	162 [10]			

[1] Langer *et al.* (1997), [2] Watanabe (1982), [3] Taran *et al.* (1994), [4] Sato – Akimoto (1979), [5] Burns (1987), [6] Hazen – Finger (1982), [7] Meagher (1975), [8] Smith – Langer (1983), [9] Hazen – Finger (1978), [10] Leger *et al.* (1990)

ground" towards the UV, type of distribution function used to model the band shape of the component bands.

A problem in the interpretation of spectra is that the influence of wavenumber-dependent light scattering, especially in the UV, is unknown so far. Currently, we are running a project on this basic problem.

Acknowledgments. First of all, I thank all the diploma and doctoral students as well as the coworkers and colleagues who decided to co-operate in the fascinating field outlined in this paper. Vicarious for all of these, I want to thank here Prof. I. Abs-Wurmbach, who was the first to work with me in this field, at that time in Bochum. My sincere thanks are alo due to Dr. Galbert, ZELMI TU Berlin, for many microprobe analyses, and to members of the staff of the Institut für Mineralogie und Kristallographie, now part of the Intitut für Angewandte Geowissenschaften I, TU Berlin, namely to S. Freitag for orientation of crystals by X-ray diffraction methods, to H. Reuff for careful preparation of oriented crystal platelets from the pre-oriented crystals, and to M. Hellwig and – later – to H. Winkelmann for continuously and relibly maintaining the institute's high pressure laboratory where synthesis and growth of crystals at high pressures and high temperatures was performed. My thanks are also due to the Technische Universität Berlin for financing the making-up of the just mentioned high pressure laboratory and for continuous help in the administration of funds from other institutions.

These are the Deutsche Forschungsgemeinschaft, Bonn-Bad Godesberg who made available our microscope-spectrometric instruments and generously supported the projects in this field. Since more than a decade, she supports by means of research stipendiates, an intense and fruitful co-operation with the research groups of Prof. Platonov, Kyiv, and of Prof. Urusov and Dr. Khisina, Moscow. The Alexander von Humboldt-Stiftung, Bonn-Bad Godesberg, generously awarded a research price to Prof. Platonov, Kyiv, and research stipendiats to Dr. Khomenko, Kyiv, and Dr. Wildner, Vienna. The co-operation was and is also supported by INTAS, Brussles, in the context of two co-operative projects run by research groups in London (Price), Paris (Calas), Kyiv (Platonov), Moscow (Uruov, Khisina) and Berlin (K. L.). To all these institutions my sincere thanks are due.

Submitted February 11, 2000

References

Abs-Wurmbach, I. – Langer, K. – Seifert, F. – Tillmanns, E. (1981): The crystal chemistry oif (Mn^{3+},Fe^{3+})-substituted andalusites (viridines and kanonaite), $(Al_{1-x-y}Mn_x^{3+}Fe_y^{3+})_2[OlSiO_4]$: crystal structure refinements, Mössbauer, and polarized optical absorption spectra. – Z. Kristallogr., 155, 81–113

Abs-Wurmbach, I. – Langer, K. – Oberhänsli, R. (1985): Polarized absorption spectra of single crytals of the chromium bearing clinopyroxenes kosmochlore and Cr-aegirine-augite. – N. Jb. MIer. Abh., 152, 293–319

Abu-Eid, R. M. (1976): Absorption spectra of transition metal-bearing minerals at high pressures: – In: Strens, R. G. J. ed: The physics and chemistry of rocks and minerals. – Wiley, New York, 641–675

Abu-Eid, R. M. – Burns, R. G. (1976): The effect of pressure on the degree of covalency of the cation-orygen bond in minerals. – Amer. Mineral., 61, 391–397

Amthauer, G. – Rossman, G. R. (1984): Mixed valence of iron in minerals with cation clusters. – Phys. Chem. Minerals, 11, 37–51

Boström, D. (1987): Sigle-crystal X-ray diffraction studies of synthetic Ni-Mg olivine solid solutions. – Amer. Mineral., 72, 965–972

Bragg, W. L. – Brown, G. B. (1926): Die Struktur des Olivins. – Z. Kristallogr., 63, 538–556

Burns, R. G. (1966): Apparatus for measuring polarized absorption specttra of small crystals. – J. Sci. Instruments, 43, 58–60

Burns, R. G. (1970): Mineralogical applications of crystal field theory. – Cambridge University Press, Cambridge

Burns, R. G. (1982): Electronic spectra of minerals at high pressures: How the mantle excites electrons. – In: Schreyer, W. ed.: High-pressure researches in geosciences. – Schweizerbart, Stuttgart, 223–246

Burns, R. G. (1987): Polyhedral bulk moduli from high-pressure crystal field spectra. In: Maghnani, M. N. and Syono, Y. eds.: High pressure research in mineral physics. – Terrapubl., Tokyo, 361–369

Burns, R. G. (1993): Mineralogical applications of crystal field theory. – Cambridge University Press, Cambridge, 2nd ed.

Burns, R. G. – Clark, J. R. – Fyfe, W. S. (1964): Crystal field theory and applications to problems in geochemistry. – In : Vinigradov, V. ed.: Chemistry of the earth's crust. – Proc. Vernadsky Centen. Symp. 2, 88–106

Čemić, L. – Grammenopoulou-Bilal, St. – Langer, K. (1986): A microscope-spectrometric method for determining small Fe^{3+}-concentrations due to Fe^{3+}-bearing defects in fayalite. – Ber. Bunsenges. Phys. Chem., 90, 654–661

Chopin, C. – Langer, K. (1988): Fe^{2+}-Ti^{4+} charge transfer between face-sharing octahedra: Poarized absorption spectra and crystal chemistry of ellenbergerite. – Bull. Minéral., 111, 17–27

Corin, F. (1931): Spectre d'absorption de la viridine. – Bull. Sopc. Geol. Belgique, 44, 313–315

Dunn, T. – McClure, D. S. – Pearson, R. G. (1965): Some aspects of crystal field theory. – Harper and Row, New York

Dyar, M. D. – Kahlenberg, V. – Langer, K. – Terzenbach, H. (1996): Polarized single cystal spectra of natural and reheated olivines in the near ultraviolet spectral region and the problem of Fe^{3+}-bearing structural defects. – Phys. Chem. Minerals., 23, 285–286

Frentrup, K. R. (1980): Absorptionsspektren von synthetischen Silikatgranaten und Granatmischkristallen und ihre Anwendung zur spektroskopische, 3d-Ionenanalyse in Granaten. Dr.-Dissertation, Universität Bonn

Frentrup, K. R. – Langer, K. (1981): Mn^{3+} in garnets: Optical absorption spectrum of a synthetic Mn^{3+}-bearing silicate garnet. – N. Jb. Miner. Mh., 245–256

Frentrup, K. R. – Langer, K. (1982): Microscope absorption spectrometry of silicate microcrystals in the range 40000–5000 cm^{-1} and its application to garnet end members synthesized at high pressures. – In: Schreyer, W. ed.: High pressure researches in geoscience. – Schweizerbart, Stuttgart, 247–258

Furche, A. – Langer, K. (1998): Polarized electronic absorption spectra of Cr_2SiO_4 single crystals. – Phys. Chem. Minerals, 25, 393–410

Garsche, M. (1994): Spektroskopische und strukturelle Untersuchungen zur intrakristallinen Ni-Mg-Verterteilung in Olivinen, $(Mg_{1-x}Ni_x)_2[SiO_4]$. – Dr.-Dissertation, Technische Universität Berlin, 150 pp.

Garsche, M. – Langer, K. (1994): Equlibrium and kinetics of cation distribution in Ni-Mg-Olivine from structure refinements and microspectrometry. – In: Putnis, A. ed.: Kinetic processes in minerals and ceramics (MINC), Poceedings of an ESF Workshop on kinetics of cation ordering, Cambridge, 5 pp.

Goldman, D. S. – Rossman, G. R. (1977): Determination of quantitative cation distributions in orthopyroxenes from electronic absorption spectra. – Phys. Chem. Minerals, 4, 43–53

Grum-Grzhimailo, V. S. (1953): Apparatus for the investigation of the colour of corundum. – Trudy Krist. Akad. Nauk SSSR, 8, 89–98

Hålenius, U. – Langer, K. (1980): Microscope-photometric methods for non-destructive Fe^{2+}-Fe^{3+} determination in chloritoids $(Fe^{2+},Mn,Mg)_2(Al,Fe^{3+})_4Si_2O_{10}(OH)_4$. – Lithos, 13, 291–294

Hålenius, U. – Annersten, H. – Langer, K. (1981): Spectroscopic studies on natural chloritoids. – Phys. Chem. Minerals, 7, 117–123

Hazen, R. M. – Finger, L. W. (1978): Crystal structures and compressibilities of pyrope and grossular to 60 kbar. – Amer. Mineral., 63, 297–303

Hazen, R. M. – Finger, L. W. (1982): Comparative crystal chemistry. Temperature, pressure, composition and the variation of crystal structure. – Wiley, New York

Hu, X. – Langer, K. – Boström, D. (1990): Polarized electronic absorption spectra and Ni-Mg partitioning in olivines $(Mg_{1-x}Ni_x)_2[SiO_4]$. – Eur. J. Mineral., 2, 29–41

Jørgensen, C. K. (1954): Studies of absorption spectra. III. Absorption bands as Gaussian error curves. – Acta Chem. Scand., 8, 1495–1501

Kersten, M. – Langer, K. – Almen, H. – Tillmanns, E. (1988): Kristallchemie von Piemontiten: Strukturverfeinerungen und polarisierte Einkristallspektren. – Z. Kristallogr., 185, 111

Khisina, N. R. – Langer, K. – Partzsch, G. (1992): Effect of Fe^{3+}-bearing point defects on the UV-spectra of two natural olivines. – Phys. Chem. Minerals, 18, 514–516

Khomenko, V. M. – Litvin, M. A. – Platonov, A. N. (1986): $Fe^{2+}Fe^{3+}$ charge transfer bands in optical spectra of amphiboles: Controlling crystallochemical factors. – Mineral Zhurnal, 8, 3–11 (in Russian)

Khomenko, V. M. – Langer, K. – Andrut, M. – Koch-Müller, M. – Vishnevsky, A. A. (1994): Single crystal absorption spectra of synthetic Ti, Fe-substituted pyropes. – Phys. Chem. Minerals, 21, 434–440

Khomenko, V. M. – Langer, K. Fett, A. (1996): Electronic absorption by Ti^{3+} and $Ti^{3+}Ti^{4+}$ charge transfer in synthetic blue rutile. – Mineral. Journ. (Kyiv), 18 (3), 12–17.

Khomenko, V. M. – Platonov, A. N. (1996): The influence of the O-O edge distance on the $Fe^{2+}\rightarrow Fe^{3+}$ charge transfer bands in amphiboles. – Phys. Chem. Minerals, 23, 243 pp.

Khomenko, V. M. – Langer, K. – Rager, H. – Fett, A. (1998): Electronic absorption by Ti^{3+} ions and electronic delocalization in synthetic blue rutile. – Phys. Chem. Minerals, 25, 338–346

Koch-Müller, M. – Abs-Wurmbach, I. – Langer, K. – Shaw, C. – Wirth, R. – Gottschalk, M. (2000): Synthetic Fe-Mg-chloritoid: structural, spectroscopic and thermodynamic studies. – Eur. J. Mineral., 12, 293–314

Kortüm, G. (1969): Reflexionsspektroskopie – Grundlagen, Methodik, Anwendungen. –Springer, Berlin

Krasovska, O. V. – Winkler, B. – Krasovskii, E. E. – Yaresko, A. N. – Antonov, V. N. – Langer, K. (1997): Ab inition calculation of the pleochroism of fayalite. – Amer. Mineral., 82, 672–676

Langer, K. (1984): Die Frabe von Mineralen und ihre Aussagefähigkeit für die Kristallchemie. – Rhein.-Westf. Akad. Wiss., Vortr. – N332, 60 pp.

Langer, K. (1988): UV to NIR spectra of silicate minerals obtained by microscope-spectrometry and their use in mineral thermodynamics and kinetics. In: Salje, E. K. H. ed. Physical properties and thermodynamic behaviour of minerals. – Reidel, Dordrecht, 639–685

Langer, K. (1999): Crystal-averaged versus local polyhedral mean distances in solid solutions - diffraction versus spectroscopy. – Eur. J. Mineral., 11 – Beih. 1, 142 pp.

Langer, K. – Abu-eid, R. M. – Anatasiou, P. (1976): Absorptionsspektren syntheticher Piemontite in den Bereichen 43000–11000 cm^{-1} (232,6–909,1 nm) und 40008–250 cm^{-1} (2,5–40 μm). – Z. Kristallogr., 144, 434–436

Langer, K. – Abu-Eid, R. M. (1977): Measurement of the polarized absorption spectra of synthetic transition metal-bearing silicate microcrystals in the spectral range 44000–4000 cm^{-1}. – Phys. Chem. Minerals., 1, 273–299

Langer, K. – Frentrup, K. R. (1979): Automated microscope-absorption spectrophotometry of rock-froming minerals in the range 40000–5000 cm^{-1} (250–2000 nm). – J. Microscopy, 116, 311–320

Langer, K. – Lattard, D. (1984): Mn^{3+} in garnets II: Optical absorption spectra of blythite-bearing, synthetic calderites, $Mn^{2+[8]}(Fe_{1-x}^{3+}Mn_x^{3+})_2^{[6]}[SiO_4]_3$. – N. Jb. Miner. Abh., 149, 129–141

Langer, K. – Hålenius, E. – Fransolet, A. M. (1984): Blue andalusite from Ottré, Venn-Stavelot Massif, Belgium: A new example of intervalence charge-transfer in the aluminium plymorphs. – Bull. Minéral., 107, 587–596

Langer, K. – Andrut, M. (1996): The crystal field concept (CFC) in geosciences: Does the crystal field stabilization energy of Cr^{3+} rule its intercrystalline partitioning behavior. – In: Dyar, M. D. – McCammon, C. – Schaefer, M. W. eds.: Mineral spectroscopy: A tribute to Roger G. Burns. – Geochem. Soc. Spec. Pub. No. 5, 29–40

Langer, K. – Taran, M. N. – Platonov, A. N. (1997): Compression moduli of Cr^{3+}-centered octahedra in some oxygen-based rock-forming minerals. – Phys. Chem. Minerals, 24, 109–114

Langer, K, – Khomenko, V. M. (1999): The influence of crystal field stabilization energy on Fe^{2+} partitioning in paragenetic minerals. – Contrib. Mineral. Petrol., 137, 220–231

Leger, J. M. – Redon, A. M. – Chateau, C. (1990): Compressions of synthethic pyrope, spessartine and uvarovite garnets up to 25 GPa. – Phys. Chem. Minerals, 17, 161–167

Lehmann, G. (1970): Ligand field and charge transfer spectra of Fe(III)-O complexes. – Z. Phys. Chem. Neue Folge, 72, 279–297

Löffler, B. M. – Burns, R. G. – Tossell, J. A. – Vaughan, D. J. – Johnson, K. H. (1974): Charge transfer in lunar materials: interpretation of ultraviolet - visible spectral properties of the moon. – Proc. 6th Lunar Sci. Conf., Geochim. Cosmochim. Acta, Suppl., 5, 3007–3016

Mao, H. K. (1976): Charge-transfer processes at high pressure. – In: Strens, R. G. J. ed.: The physics and chemistry of minerals and rocks. – Wiley, New York, 573–581

Mao, H. K. – Bell, P. M. (1971): Crystal field spectra. – Ann. Rept. Geophys. Lab., Yearb. Carnegie Inst. Wash. 70, 207–215

Marfunin, A. S. (1977): Pysics of minerals and inorganic materials. – Springer, Berlin

Matsyuk, S. S. – Langer, K. – Hösch, A. (1998): Hydroxyl defects in garnets from mantle xenoliths in kimberlites of the Siberian platform. – Contrib. Mineral. Petrol., 132, 163–179

Matsyuk, S. S. – Platonov, A. N. – Khomenko, V. M. (1985): Optical spectra and colour of mantle minerals in kimberlites. – Naukova Dumka, Kiev

Mattson S. M. – Rossman, G. R. (1987): Identifying characteristics of charge transfer transitions in minerals. – Phys. Chem. Minerals, 14, 94–99

Meagher, E. P. (1975): The crystal structure of pyrope and grossularite at elevated temperatures. – Amer. Mineral., 60, 218–228

Merlino, S. (1965): Applicazione delle teoria desl campo cristallino alla studio della riparizione di elementi in trace. – Atti della Soc. Tosc. Sci. Nat, Ser. A 72, 14 pp.

Moore, R. K. – White, W. B. (1972): Electronic spectra of transition metal ions in silicate garnets. Canad. Mineral., 11, 791–811

Nakamura, A. – Schmalzried, H. (1983): On the nonstoichiometry and point defects of olivine. – Phys. Chem. Minerals., 10, 27–37

Nassau, K. (1983): The physics and chemistry of color: The fifteen causes of color. Wiley, New York

Nitsan, U. (1974): Stability of olivine with respect to oxidation and reduction. – J. Geophys. Res., 79, 706–711

Peckett, A. (1992): The colours of opaque minerals. – Wiley, New York

Piller, H. (1977): Microscope photometry. – Springer, Berlin

Platonov, A. N. (1976): The nature of the colour of minerals. – Naukova Dumka, Kiev – 262 pp. (in Russian)

Platonov, A. N. – Langer, K. – Matsyuk, S. S. – Taran, M. N. – Hu, X. (1991): Fe^{2+}-Ti^{4+} charge-transfer in garnets from mantle eclogites.– Eur. J. Mineral., 3, 19–26

Platonov, A. N. – Langer, K. – Chopin, C. – Andrut, M. – Taran, M. N. (2000): Fe^{2+}-Ti^{4+} charge-tranfer in dumortierites. – Eur. J. Mineral., (in press)

Platonov, A. N. – Langer, K. – Wildner, M. – Polshin, E. V. – Matsyuk, S. S. (2000): The crystal chemistry of the humite minerals: Spectroscopic studies and structure refinement of an unusual iron-rich clinohumite. – Z. Kristallogr., submitted

Ramsey, D. A. (1952): Intensities and shapes of infrared absorption bands of substances in the liquid state. – J. Amer. Chem. Soc., 74, 72–80

Rossman, G. R. (1988): Optical spectroscopy. – In: Hawthorne, F. C. ed.: Spectroscopic methods in mineralogy and geology. – Rev. Min., 18, 207–254

Sato, Y. – Akimoto, S. (1979): Hydrostatic compression of four corundum-type compounds: α-Al_2O_3, V_2O_3, Cr_2O_3 and α-Fe_2O_3. – J. Appl. Phys., 50, 5285–5291

Sherman, D. M. (1984): The electronic structures of manganse oxide minerals. – Amer. Mineral., 69, 788–799

Sherman, D. M. (1987a): Molecular orbital (SCF-Xα-SW) theory of metal-metal charge transfer processes in minerals. I. Application to $Fe^{2+} \rightarrow Fe^{3+}$ charge-transfer and "electron delocalization" in mixed valence iron oxides and silicates. – Phys. Chem. Minerals, 14, 355–363

Sherman, D. M. (1987b): Molecualer orbital (SCF-Xα-SW) theory of metal-metal charge transfer processes in mineral. II. Application to $Fe^{2+} \rightarrow Ti^{4+}$ charge transfer transitions in oxides and silicates. – Phys. Chem. Minerals, 14, 364–367

Smith, G. – Strens, R. G. J. (1976): Intervalence transfer absorption in some silicate, oxide and phosphate minerals. – In: Strens, R. G. J. ed.: The physics and chemistry of minerals and rocks, Wiley, New York, 583–612

Smith, G. – Langer, K. (1981): Polarized single-crystal Near UV spectra of synthetic olivines. – Naturwiss., 67, 373

Smith, G. – Langer, K. (1982 a): Single crystal spectra of olivines in the range 40000–5000 cm^{-1} at pressures up to 200 kbar. – Amer. Mineral., 67, 343–348

Smith, G. – Langer, K. (1982 b): High pressure spectra of olivines in the range 40000–11000 cm^{-1}. - In: Schreyer, W. ed.: High pressure researches in geoscience. – Schweizerbart, Stuttgart, 259–268

Smith, G. – Langer, K. (1983): High pressure spectra up to 120 kbar of the synthetic garnet end members spessartine and almandine. – N. Jb. Miner. Mh., 541–555

Sockel, H. G. (1974): Defect structure and electrical conductivity of crystalline ferrous silicate. – In: Seltzer, M. S. – Jaffe, R. I. eds.: Defects and transport in oxides. Plenum Press, New York, 341–354

Steffen, G. – Langer, K. – Seifert, F. (1988): Polarized electronic absorption spectra of synthetic (Mg,Fe)-orthopyroxenes, ferrosilite and Fe^{3+}-bearing ferrosilite. – Phys. Chem. Minerals, 16, 120–129

Tanabe, Y. – Sugano, S. (1954a and b): On the absorption spectra of complex ions. I. and II. – Journ. Phys. Soc. Japan), 753–766 and 767–779

Taran, M. N. – Langer, K. – Platonov, A. N. – Indutny (1994): Optical absorption investigation of Cr^{3+}-ion bearing minerals in the temperature range 77–797 K. Phys. Chem. Minerals, 21, 360–372

Taran, M. N. – Langer, K. – Platonov, A. N. (1996): Pressure- and temperature effects on exchange-coupled pair bands. – Phys. Chem. Minerals., 23, 230–236

Taran, M. N. – Langer, K. (1998): Temperature and pressure dependence of intervalence charge transfer bands in spectra of some Fe- and Fe, Ti-bearing oxygen-based minerals. – N. Jb. Miner. Abh., 172, 325–346

Taran, M. N. – Langer, K. (2000): Electronic absorption spectra of Fe^{3+} ions in andradite and epidote at different temperatures and pressures. – Eur. J. Mineral., 12, 7–15

Tossell, J. A. (1976): Electronic structures of iron-bearing oxidic minerals at high pressures. – Amer. Mineral., 61, 130–144

Tossell, J. A. – Vaughan, D. J. – Johnson, K. H. (1974): The electronic structure of rutile, wustite and hematite from molecular orbital calculations. – Amer. Mineral., 59, 319–334

Urusov, V. S. (1992): A geometric model for deviations from Vegrd's rule. – J. Solid State Chem., 98, 223–236

Vaughan, D. J. – Tossell, J. A. – Johnson, K. H. (1974): The bonding of ferrous iron to sulfur and oxygen in tetrahedral coordination: a comparative study using SCF Xα scattered wave molecular orbital calculations. – Geochim. Cosmochim. Acta, 38, 993–1005

Watanabe, T. (1982): Thermodynamic properties of synthetic high-pressure compounds relevant to the earth's mantle. – In: Maghnani, M. H. – Akimoto, S. eds.: High-pressure research in geophysics. – Ceter Acad. Publ., Tokyo, 441–464

Wildner, M. – Langer, K. (1994): Polarized electronic absorption spectra of $3d^3$-configurated tetravalent manganese in octahedral fields of $Mn(SeO_3)_2$. – Phys. Chem. Minerals, 21, 294–298

Wildner, M. – Langer, K. (1994): Co^{2+} in trigonal fields of oxygen based structures: Electronic absorption spectra of buetschliite-type $K_2Co(SeO_3)_2$, $K_2Co_2(SeO_3)_3$ and zemannite-type $K_2Co_2(SeO_3)_3 \cdot 2H_2O$. – Phys. Chem. Minerals, 20, 460–468

Nový pohled mikroskopem – lokálně rozlišená elektronová absorpční spektra silikátů měřená mikroskopem-spektrometrem

Článek diskutuje koncepty absorpční spektroskopie ve vlnových spektrech W, VIS a MR a excitaci elektronových přechodů v oxysolích v těchto vlnových rozmezích. Absorpce energie v tomto rozmezí vzbuzuje přechody v elektronových systémech ligandu a centrálních iontů v polyedrech, LM-CT, v elektronových systémech dvou $3d^N$-iontů s různými valencemi umístěnými v propojených polyedrech, MM-CT, a mezi energetickými stavy $3d^N$-iontu samotných, dd-sa a dd-sf. Teoretické aspekty těchto přechodů a jejich zhodnocení, která přinášejí četné informace užitečné v krystalové chemii a krystalové fyzice minerálů, jsou stručně uvedeny. Jsou diskutovány mikroskopické-spektrometrické metody vyvinuté za účelem překonání obtíží, spojených s častou potřebou skanovat spektra malých krystalků, malých opticky čistých částí větších krystalů, nebo omezit pozorování na průměr malých apertur speciálních instrumentací, jako jsou vysokotlaké DAC cely, vysokoteplotní cely a podobně. Tyto metody umožňují měření na vybraných místech kolem pouhých 5 μm v průměru; lze získat polarizovaná spektra v širokém rozmezí od 40000 do 5000 cm^{-1} (250 až 2000 nm) při tlaku ≤20 GPa a při teplotách mezi 100 a 900 °K. Jsou uvedeny příklady úspěšných aplikací těchto metod na problémy barvy minerálů, interpretace absorpcí v komplexních minerálech studiem chemicky jednoduchých syntetických analogů, chemické analýzy včetně Fe^{2+} a Fe^{3+}, vnitrokrystalové a mezikrystalové distribuce 3dN iontů a analýzy lokálních strukturních vlastností polyedrů centrovaných na 3dN-ionty. Lokální strukturní zvláštnosti nemohou být objasněny difrakčními metodami strukturního výzkumu, které pracují na základě průměrování struktury a nemohou „vidět" polyedry s 3dN-ionty individuálně. Z tohoto oboru diskutujeme analýzu Fe^{3+}-obsahujících defektů ve fayalitu a olivínech, produkovaných v závislosti na fO_2 a teplotě. Výsledků tohoto studia mohou být použity k odhadu fugacity kyslíku v přírodních procesech. Pojednáváme rovněž o zhodnocení pruměrných lokálních vzdáleností $3d^N$-iontů a ligandu individuálních polyedrů centrovaných na $3d^N$-iontech, a o stanovení stlačitelnosti a termální roztažnosti polyedru.